NR2F2 Reactivation in Early-life Adipocyte Stem-like Cells Rescues Adipocyte Mitochondrial Oxidation

Snehasis Das[1], Rohan Varshney[1], Jacob W. Farriester[1], Gertrude Kyere-Davies[1], Alexandrea E. Martinez[1], Kaitlyn Hill[1], Michael Kinter[2], Gregory P. Mullen[1], Prabhakara R. Nagareddy[3], Michael C. Rudolph*[1]

[1]Department of Biochemistry and Physiology, Harold Hamm Diabetes Center, The University of Oklahoma Health Science Center, Oklahoma City, OK 73104, USA.

[2]Aging and Metabolism Research Program, Oklahoma Medical Research Foundation, Oklahoma City, OK.

[3]Deptartment of Internal Medicine, Cardiovascular Section, The University of Oklahoma Health Science Center, Oklahoma City, OK 73104, USA.

Keywords: NR2F2, early-life adipocyte development, omega-3 fatty acids, adipocyte stem-like cells, beige adipocyte metabolism

*Corresponding author: Dr. Michael C. Rudolph, Email- Michael-rudolph@ouhsc.edu

ABSTRACT

In humans, perinatal exposure to an elevated omega-6 (n6) relative to omega-3 (n3) Fatty Acid (FA) ratio is associated with the likelihood of childhood obesity. In mice, we show perinatal exposure to excessive n6-FA programs neonatal Adipocyte Stem-like cells (ASCs) to differentiate into adipocytes with lower mitochondrial nutrient oxidation and a propensity for nutrient storage. Omega-6 FA exposure reduced fatty acid oxidation (FAO) capacity, coinciding with impaired induction of beige adipocyte regulatory factors PPARγ, PGC1α, PRDM16, and UCP1. ASCs from n6-FA exposed pups formed adipocytes with increased lipogenic genes in vitro, consistent with an in vivo accelerated adipocyte hypertrophy, greater triacylglyceride accumulation, and increased % body fat. Conversely, n6-FA exposed pups had impaired whole animal ^{13}C-palmitate oxidation. The metabolic nuclear receptor, NR2F2, was suppressed in ASCs by excess n6-FA intake preceding adipogenesis. ASC deletion of NR2F2, prior to adipogenesis, mimicked the reduced FAO capacity observed in ASCs from n6-FA exposed pups, suggesting that NR2F2 is required in ASCs for robust beige regulator expression and downstream nutrient oxidation in adipocytes. Transiently re-activating NR2F2 with ligand prior to differentiation in ASCs from n6-FA exposed pups, restored their FAO capacity as adipocytes by increasing the PPARγ-PGC1α axis, mitochondrial FA transporter CPT1A, ATP5 family synthases, and NDUF family Complex I proteins. Our findings suggest that excessive n6-FA exposure early in life dampens an NR2F2-mediated induction of beige adipocyte regulators, resulting in metabolic programming that is shifted towards nutrient storage.

INTRODUCTION

The prevalence of obesity in children and adolescents in the United States is approaching 20%, and approximately 40% of U.S. children are either overweight or obese[1]. Predictions suggest that half of American children may reach clinical obesity by age 35[2], underscoring the urgency of this public health crisis. The onset of obesity is not only occurring at younger ages but is frequently accompanied by a range of comorbidities typically associated with adulthood, such as non-alcoholic fatty liver, type 2 diabetes, cardiovascular disease, psycho-social consequences, and even premature mortality[3-5]. Although obesity has a complex etiology, including genetic, epigenetic, environmental, and behavioral characteristics, emerging evidence points to early-life nutrition as central to obesity risk, not merely as substrates and fuels for fetal and postnatal development, but as programming cues that can establish enduring consequences for adult metabolism[6-10]. For example, maternal intake of a Western-style diet, rich in omega-6 fatty acids (n6-FA) and processed sugars, has been implicated in metabolic programming changes in offspring, potentially increasing risks for non-communicable metabolic diseases[3]. In recent years, the balance of dietary lipids consumed by pregnant and lactating mothers has come into focus, particularly the ratio of pro-adipogenic n6-FA relative to anti-adipogenic omega-3 (n3) FA [11-14].

Maternal transmission of a high ratio of n6/n3 FA to offspring is recognized for its influence in shaping adipocyte development and adipose tissue accumulation[11,12,15-18]. Our research, and that of others, shows that a high n6/n3 FA ratio in breast milk accelerates infant body fat deposition and increases the likelihood of greater childhood adiposity[18-24]. For example, in a cohort of 48 exclusively breastfeeding mother infant dyads, we showed an elevated n6/n3 FA ratio in the milk predicted the change in infant body fat accumulation in the first four months of life, controlling for maternal prepregnancy BMI, fish oil supplementation, gestational weight gain, infant sex, and breastfeeding exclusivity[25]. In neonates particularly, adipose tissue is not merely a nutrient-storage reservoir of lipid-laden adipocytes[26], it is a critical

metabolic and signaling organ that contributes to thermogenesis, through nutrient oxidation, to defend the body temperature of offspring[27-29]. Consistent with our human infant findings, we reported that mouse pups exposed to n6-FA during the fetal and postnatal window had greater body fat at postnatal day (PND) 14, and an inguinal subcutaneous adipose tissue (SAT) with larger, unilocular adipocytes, indicating a nutrient storage phenotype[30]. Molecularly, a high n6/n3 FA ratio exposure increased master adipogenic regulator Peroxisome Proliferator Activated Receptor gamma (PPARγ), lipogenic enzyme mRNA and protein levels, and produced an activated mRNA signature for the "adipogenesis pathway" [30].

Adipocyte Stem-like Cells (ASCs) commit to become determined preadipocytes, and then terminally differentiate, giving rise to functional adipocytes[31-35]. More recently, we investigated whether a high n6/n3 FA ratio exposure, specifically during postnatal development, affected adipogenesis by patterning the molecular signature of Adipocyte Stem-like Cells (ASCs)[36]. Through bulk and single-cell RNA-sequencing analyses, we found ASCs from high n6/n3 FA ratio exposed pups had an inhibited b-Catenin (CTNNb1) and Wingless-type MMTV integration site (WNT) mRNA signature, and significantly decreased mRNA and protein levels of Nuclear Receptor 2 group F member 2 (NR2F2, also known as COUP-TF2) [36]. NR2F2 is a ligand-activated transcription factor that is known to be induced by activation of the WNT/CTNNb1 signaling pathway in 3T3L1 preadipocyte cells[37,38]. NR2F2 plays a pivotal role in regulating metabolism across various tissues, by either activating or repressing transcription through direct DNA binding or dimerization with other nuclear receptors [39-44]. For example, NR2F2 interaction with PPARα regulates lipid metabolism in the liver, where NR2F2-PPARa cooperativity mediates expression of fatty acid oxidation (FAO) target genes [45]. Others showed that NR2F2 can bind PPARg, or sequester binding partners such as RXR away from PPARg[46]. We reported distinct ASC responses to *in vivo* n6-FA exposure, in that isolated inguinal SAT ASCs had altered mitochondrial gene expression patterns, fewer "mitochondrial-high" ASCs, and reduced FAO prior to differentiation, which coincided with increased fat mass and larger,

unilocular nutrient-storing adipocytes[36].

Given these early-life high n6/n3 FA ratio effects on inguinal ASCs, we hypothesize that fetal and postnatal exposure to high n6-FA levels trigger ASCs to differentiate into nutrient-storing rather than nutrient-oxidizing adipocytes, which might be overcome by activating NR2F2. We provided pregnant and lactating dams with a specialized diet rich in n6-FA relative to dams provided a balanced, control-FA specialized diet to test the molecular signatures, adipocyte cellular fuel utilization, whole-body metabolic responses, and whether activation of NR2F2 could rescue adipocyte metabolism in ASCs programmed in vivo by n6-FA exposure in PND12 pups. Our findings indicate that in undifferentiated ASCs, NR2F2 acts upstream to establish key regulators of nutrient-oxidizing adipocytes. Furthermore, transient activation of NR2F2 in ASCs isolated from n6-FA exposed pups reignited nutrient-oxidizing metabolism, in part, by restoring mitochondrial protein levels. Our data suggest a model whereby early-life n6-FA exposure limits WNT/CTNNb1 activation, diminishing NR2F2 abundance and robust induction of metabolic regulators, resulting in formation of nutrient-storing adipocytes.

MATERIALS AND METHODS

Mouse study: Animal procedures were approved by the IACUC at the University of Oklahoma Health Sciences Center. Wildtype C57BL/6J mice were purchased from Jackson Laboratories (Bar Harbor, MN, USA). The study design used wildtype mothers to assess the effect of different PUFA ratio exposures on offspring development. Prospective dams were provided with the control diet until mating, during which they were divided into control (balanced n6/n3 ratio) and n6-FA (high n6/n3 ratio) groups, provided with appropriate diets, and underwent normal gestation and lactation. At PND12, litters were assessed for body composition, and pups were sacrificed for histology, collection of stromal vascular fractions (SVF), ASC flow cytometry, and

assessment of gene expression, protein levels, and circulating hormones, glucose, and fatty acid composition.

Body composition and indirect calorimetry. Body composition was assessed using quantitative magnetic resonance (qMR; Echo MRI Whole Body Composition Analyzer 4in1-500; Echo Medical Systems, Houston, TX, USA) on PND 12 for dams and litters, as previously described [30]. Individual litters were weighed before undergoing three consecutive body composition scans, and averages of returned values for fat and lean mass were utilized for analysis.

Dam-litter dyads were placed in indirect calorimetry (IDC, Sable Systems International, Las Vegas, Nevada) cages housed inside the environmental cabinet maintained at 26°C at PND 10. On PND 11, dams were separated from their respective litters for 2 hours, placed back with their litters for 1 hour, then removed from their litters again for 3 hours before finally being placed back with their litters until PND 12. The litters were weighed and body composition measured before the first and second separation of the dam using a weigh-suckle-weigh paradigm to estimate the amount of milk consumed by the pups during the 1 hour feeding window. During the period from PND 10 to PND 12, the dyads (and isolated litters intermittently during weigh-suckle-weigh) in the IDC were monitored for metabolic parameters, including respiratory exchange ratio (RER).

In separate experiments, independent dam-litter dyads were placed in IDC chambers at PND 10. At PND 11, litters were gavaged with 500µg (50µL) of uniformly ($^{13}C_{16}$) labeled palmitate (dissolved in peanut oil). The dam was separated from the pups for four hours, during which litter respirometry was measured in the IDC to analyze the amount of labeled (^{13}C) CO_2 exhaled by the litter per minute using a stable isotope analyzer (Sable Systems International). This gave a measure of palmitate oxidation by the litters. Litters were euthanized on PND 12, and tissues collected to measure the $^{13}C_{16}$ palmitate uptake by GC-MS.

Histology and Immunohistochemistry (IHC). Histological blocks were prepared from Subcutaneous White Adipose Tissue (SAT). Inguinal SAT pads were gathered from perinatal (PND 10–13) mice, fixed in 10% neutral buffered formalin (NBF), rinsed, and stored in 70% EtOH, and embedded in paraffin. Slides mounted with 5–10 µm sections were analyzed using Immunohistochemistry (IHC) and Hematoxylin and Eosin (H&E) staining. Brightfield and Immunofluorescence whole-slide imaging was conducted using a ZEISS Axio Scan. Z1 Slide Scanner, and composite images were compiled using Zeiss's Zen Blue software.

Slides used for Hematoxylin and eosin (H&E) staining were prepared following the standard Leica Biosystems' "Best Practices" protocol. Quantification of adipose cellularity was accomplished through digital analysis of scanned histological sections using the Adiposoft plugin[47,48] for ImageJ/Fiji[49]. Brightfield whole-tissue scans of H&E-stained slides were optimized for ImageJ processing—including sharpening/clarification and masking of nontarget tissues to reduce artifacts—using Adobe Photoshop. Adipocyte cellularity (diameter, µm) was quantified from each optimized section with Adiposoft. After manually removing any remaining Adiposoft artifacts from the output data, diameter values within a set threshold (15–200 µm) were binned and imported into GraphPad PRISM, where the percentage of adipocytes within each bin was analyzed.

Slides for IHC staining were processed following a standard multi-color immunofluorescence staining protocol[50,51] and counterstained with DAPI (200 ng/mL). For each sample, multi-channel, shading-corrected images rendered by ZEN Blue were exported into Adobe Photoshop for preparation for image analysis. The tissue sample was isolated from the composite scan by masking background space, nontarget tissues, and instances of highlight clipping, using DAPI and Perilipin-1-stained area for reference when demarking tissue boundaries. Final images used for quantitative analysis were rendered by applying this mask to each color channel image. Additional images were rendered from masked composite scans by creating separate masks that visually isolated beige and white adipose tissue, allowing relative

intensity to be quantified independently. Using ImageJ, relative intensity of each fluorophore was determined by finding the quotient of the total area of the tissue sample and the integrated density (the product of the area and the mean grey value, or average gray value of pixels, within a selection) of fluorescence.

Primary antibodies used on SAT sections for IHC were UCP1 (1:200) and Rabbit Perilipin-1 mAb (1:500). Secondary Antibodies utilized were Alexa Fluor 594 Anti-Rat IgG, Alexa Fluor 594 Anti-Rabbit IgG, and Alexa Fluor 488 Anti-Rabbit IgG. Alexa Fluor 594 was analyzed for relative intensity quantification. Adipocytes within white and beige tissue were quantified by exporting the DAPI-Channel image with phenotype masks applied into ImageJ and analyzing using the built-in "Analyze Particles" function. From this, cell density (nuclei/μm^2) was found by dividing the nuclei count by the area of the target tissue.

Flow cytometry sorting and analysis. Flow sorting and analyses were performed as previously described[36]. Briefly, subcutaneous adipose tissue was minced and digested in Hanks Balanced Salt Solution (HBSS) (Sigma, H8264) containing 3% BSA, 0.8 mg ml^{-1} collagenase type 2 (Worthington Biochemical, LS004174), 0.8 mM $ZnCl_2$, 2.5 mM glucose and 0.2 µM adenosine for 45 minutes at 37°C in an orbital shaker at 150 RPM, and samples were shaken vigorously by hand for one minute after digestion. The resulting suspension was filtered through a 70µm filter. Cells in the stromal vasculature fraction were pelleted at 300xg, washed with HBSS buffer containing 3% BSA, and stained with primary antibodies on ice for 30 minutes. The following antibodies were used: CD45 FITC at 1:1,000 (BioLegend; 103108), CD31 PE-Cy7 at 1:500 (BioLegend, 102417), CD29 Alexa Fluor 700 at 1:200 (BioLegend, 102218), CD34 APC at 1:50 (BioLegend, 119310), Sca-1 BV510 at 1:200 (BioLegend, 108129), and CD24 PE at 1:100 (BioLegend, 138504). Following antibody incubation, cells were washed, and unfixed cell preparations were treated with DAPI (Invitrogen) at 1µg/ml to exclude dead cells. Cells were sorted using a FACS Aria Fusion equipped with FACS DiVA software (BD Biosciences) using a

specific gating strategy (Suppl Fig 2). Cell populations were selected based on forward scatter (FSC) and side scatter (SSC), and dead cells were excluded. Single cells were isolated or analyzed based on cell surface markers. Data was analyzed using BD FACS DiVA and FlowJo.

Cell culture and differentiation. The immortalized adipocyte precursor (mAPC) cell line was purchased from Kerafest (MA, USA). mAPCs were cultured in High Glucose Dulbecco's Modified Eagle Medium 1:1 with Hams F-12 (DMEM/F12) containing 10% FBS supplemented with penicillin (100 U/mL) and streptomycin (100 µg/mL) at 37℃ in a humidified incubator with 5% CO_2. Primary ASCs were cultured under similar conditions in High Glucose Dulbecco's Modified Eagle Medium (DMEM) containing 10% fetal bovine serum (FBS) supplemented with penicillin and streptomycin. For differentiating cells into beige adipocytes, mAPCs and ASCs were cultured in their respective mediums until nearly confluent and the medium was then changed to induction medium (5 µg/mL insulin, 1 nM T3, 125 µM indomethacin, 2 µg/mL dexamethasone, 0.5 mM IBMX, 0.5 µM rosiglitazone) when cells are 80-90% confluence (day 2). After 48h (Day 4), the medium was changed to maintenance medium (5 µg/mL insulin, 1 nM T3) with 0.5 µM rosiglitazone). On day 6 and 8, spent medium was replaced with fresh maintenance medium with 1 µM rosiglitazone. On termination of differentiation at day 10, cells were utilized for the various assays described herein. For some experiments, 1-DSO (300 nM) was added to ASCs and mAPCs for four days flanking induction (two days before the induction to two days after). This is depicted schematically in the figures.

For NR2F2 knockdown experiments, ASCs isolated from $NR2F2^{f/f}$ mice were transduced with adeno-Cre (AdCre) or adeno control (AdCon) virus. 5-6 days after transduction, the cells were treated with induction media to initiate differentiation. For other experiments, 70-80% confluent ASCs from n6-FA pups were treated with Wnt agonist 1 for 48h to induce Wnt-CTNNb1 pathway.

Live cell staining for mitochondrial potential, fatty acid oxidation, and lipid accumulation Primary ASCs were cultured as described above. For staining with tetramethylrhodamine ethyl ester (TMRE, Biotium) live cell mitochondrial potential dye and LipidSpot™ 488 (Biotium), media were changed to fresh DMEM/10% FBS containing these stains diluted 1:1,000. Cells were incubated at 37℃ for 15 minutes before fluorescent data was collected using a Zoe™ Fluorescent Cell Imager (BioRad). For staining with FAOBlue (Funakoshi), TMRE, and LipidSpot 488, cells were washed twice in serum-free DMEM and then incubated for 15 min. at 37℃ in fresh DMEM (no serum) containing FAOBlue (1:1,000). TMRE and LipidSpot™ 488 were added and cells incubated 15 min. at 37℃ before imaging.

Quantitative PCR and Western blotting. Total RNA was extracted using the RNeasy Plus Mini Kit (Qiagen, Hilden, Germany, 74134) according to the manufacturer's protocol, and 500ng of total RNA was reverse transcribed into cDNA using iScript Reverse Transcription Supermix (Bio-Rad, Hercules, CA, USA) or the Verso cDNA Synthesis Kit (ThermoFisher, MA, USA). cDNA representing 25ng of total RNA was added to each qPCR reaction containing TaqMan Fast Advanced Master Mix and primers (ThermoFisher, MA, USA) specific for Pparγ, Pgc1α, Ucp1, PRDM16, Cidea, Cox8b, Cox7a1, Acly, Acc1, Fasn, Srebp1, Srebp2, Dgat1, or Nr2f2 were used for quantitative real time PCR (Applied Biosystem, 589 Ca, USA). Ef1α was used as a housekeeping gene. mRNA levels were determined using the ΔΔCT method and normalized to the housekeeping gene Ef1α.

For Simple Westerns using JESS, flow-sorted primary ASCs, mature adipocytes or whole iWAT were homogenized in RIPA buffer with protease and phosphatase inhibitors. Lysates were run on a ProteinSimple JESS instrument for PPARγ (CST- 2435), PGC1α (CST-2178), C/EBPα (CST- 2295), UCP1 (CST- 14670), CPT1A (Protein Tech- 15184-1-AP), CPT1C (Protein Tech- 12969-1-AP), FABP4 (CST- 2120), NR2F2 (CST- 6434), SOD2 (CST-13141), TOM20 (CST- 42406), and PLIN1 (CST- 9349) antibodies. All antibodies were diluted 1:50 and

3 µL of 1.2mg/ml protein/well was loaded for JESS Westerns. Protein from primary ASCs from six different SVFs for each dietary condition (high n6 or control) were used for each JESS assay.

Seahorse Cellular Metabolic Assays. Seahorse substrate oxidation assays were conducted using the manufacturer's instructions with some modifications described below, utilizing the glucose/pyruvate oxidation stress test kit (103673-100), glutamine oxidation stress test kit (103674-100), and palmitate oxidation stress test kit (103693-100). Modifications include adding inhibitors (20µL per well) directly to the cells both 15 minutes before the assay and following the standard mito stress test protocol.

Targeted Lipid Analysis. 500µL of 0.1M potassium phosphate buffer, pH 6.8 was added to 13x100mm borosilicate glass culture tubes (Fisher Scientific, #14-961-27), to which 6µL of pup serum was added. The mixture was then acidified with 10µL of 1N HCl (prewashed with Hexanes) and vortexed briefly. 500µL of methanol was added to this solution and vortexed briefly. Total lipids were extracted twice by adding 1mL of isooctane:ethyl acetate 3:1 (vol/vol) and once with 1mL Hexane; for each extraction, samples were vortexed vigorously for 10-15 sec and centrifuged at 2000g for 1 minute to complete phase separation. The organic layer from each extraction was combined into a new 13x100 mm borosilicate glass tube. Extracted lipids were brought to dryness and resuspend in 300µL 2,2,4-Trimethylpentane (isooctane). For the non-esterified fatty acid (NEFA) fraction, 100µL of resuspended total lipids was transferred to a new borosilicate glass tube, mixed with (25 ng) blended stable isotope internal standard, taken to dryness under gaseous N_2, and resuspended in 25µL of 1% pentafluorobenzyl bromide in acetonitrile (vol/vol), to which 25µL of 1% diisopropylethylamine in acetonitrile (vol/vol) was added, and samples were incubated at room temperature for 30 minutes. Pentafluorobenzyl-fatty acid derivatives were taken to dryness under gaseous N_2 and resuspended in 100µL hexane for injection into the GC/MS. For the total fatty acid fraction (TFA), 50µL of the original

300µL total lipid extract was transferred to a separate Teflon lined screw cap glass tube, mixed with (66.7 ng) blended stable isotope internal standard, and taken to dryness under gaseous N_2. TFA samples were resuspended in 500µL of 100% ethanol, to which 500µL of 1M NaOH was added to saponify the TFA fraction at 90°C for 30 minutes, followed by acidification using 550µL of 1M HCl. Saponified samples were then extracted twice with 1.5mL of Hexanes, taken to dryness under gaseous N_2, and derivatized as above. Derivatized TFA samples were resuspended in 267µL hexanes for injection into the GC/MS. For $^{13}C_{16}$-palmitate measurement in tissues from tracer gavaged pups, the tissues were homogenized in a bead mill (Fisher Scientific) in 2mL bead mill tubes in 1mL of 66% methanol (in pH 6.8 KPhos buffer). The homogenates were transferred to 13x100mm borosilicate glass tubes and 40µL of prewashed HCl was added mixed briefly. Lipids were extracted as above and reconstituted in 300µL Isooctane. 50µL of resuspended total lipids was transferred to a new Teflon lined screw cap glass tube, mixed with (66.7 ng) $^{2}D_{31}$-palmitate internal standard and taken to dryness under gaseous N_2. Samples were saponified, extracted, and derivatized as above. Derivatized samples were resuspended in 267µL hexanes for injection. For the NEFA, TFA and tracer fractions, 1µL of pentafluorobenzyl-fatty acid derivatives was injected and data were collected on the GC-MS (8890 GC, 5977B MSD, Agilent) DB-1MS UI column (122-0112UI, Agilent) with the following run program: 80°C hold for 3 minutes, 30°C/minute ramp to 125°C, no hold, 25°C ramp to 320°C and hold for 2 minutes. The flow rate for the methane carrier gas was set at 1.5mL/minute. Data were acquired in full scan negative chemical ionization mode to identify fatty acids of acyl chain length from 8 to 22 carbons. Peak areas of the analyte or standard were measured, and the ratio of the area from the analyte-derived ion to that from the internal standard was calculated[52]. $^{13}C_{16}$-palmitate was analyzed relative to the quantitative $^{2}D_{31}$-palmitate internal standard[53].

Proteomics. ASCs were isolated from control and n6-FA pups and plated in 6-well plates, followed by differentiation into beige adipocytes, with or without 1-DSO exposure flanking beige induction in the n6-FA ASCs. After differentiation, cells were washed twice with PBS and lysed in 100ml RIPA buffer per well and used for proteomics.

Sample processing for proteomics: A GeLC approach was used, in which each sample was run approximately four cm into an SDS-Page gel, fixed, and stained with Coomassie blue. Each lane of the gel was cut top to bottom as a series of seven broad molecular weight fractions. ach fraction was chopped into smaller pieces, washed, reduced with DTT, alkylated with iodoacetamide, and digested with 1µg trypsin overnight at room temperature. Peptides were extracted from the gel in 50% acetonitrile, the extracts taken to dryness by Speedvac, and reconstituted in 200µL 1% acetic acid for analysis.

LC-MS for proteomics:

We used a ThermoScientific QEx Plus instrument interfaced to an Ultimate 3000 nanoflow HPLC system with 75um x 20xm C18 (Phenomenex Aeris XB-18 3.6um beads) capillary columns packed in CoAnn tips. 10uL samples are injected and loaded on the column at 1.5uL/min for 8minutes. Peptides are eluted with a linear gradient of acetonitrile in water with 0.1% formic acid from 1% to 50% in 60min at a flow rate of 150nL/min.

Data dependent acquisition (DDA)- The DDA experiments used a top 20 strategy where one full scan MS spectrum was acquired followed by 20 CID spectra. The full scan mass spectra were acquired with an m/z resolution of 70,000 and CID spectra with an m/z resolution of 17,500. Ion source settings included a spray voltage of 2.2 kV, ion transfer tube temperature of 300◦ C, and positive ions mode.

DDA data are searched against the Uniprot proteome database from Embl. Mascot matches each CID spectrum to a peptide sequence in the database, considering the digestion with trypsin, cysteine alkylation, and variable methionine oxidation. The identifications are ranked based on a total score determined by the program based on the quality and number of peptide matches. Only proteins with two or greater matching peptides are included in the results.

Enzyme linked immunosorbent assay (ELISA). ELISAs for high molecular weight (HMW) and total adiponectin (ALPCO, 47-ADPMS-E01), Acylation Stimulating Protein (ASP, MyBioSource, MBS263213), Complement C3 (Abcam, ab157711), Insulin (Crystal Chem, 90080), Leptin (R&D, DY498) and Retinol-Binding Protein 4 (RBP4, R&D, DY3476) were performed following manufacturers' instructions. Pup serum was collected from trunk blood (pooled from two to three pups per group) and diluted 1:8181, 1:200, 1:50000, 1:1, 1:1 and 1:2000 for HMW and total adiponectin, ASP, Complement C3, Insulin, Leptin and RBP4, respectively.

Statistical Analyses. Results are presented as mean ± SEM with *p* values less than 0.05 considered significantly different. Two-way ANOVA, repeated measures two-way ANOVA, one-way ANOVA, t-test, or multiple comparison t-test were performed for the analyses of differences between groups. Tukey post-hoc comparisons were done where appropriate using GraphPad Prism Software, Version 9.

DATA AVAILABILITY

Source data are provided with this paper. Source data for Figures 4L and 5H are included with this paper as source data file 1. Source data for Table 1 is included in this paper as Source data file 2. No publicly available data sets were generated or analyzed for this study.

RESULTS

Omega-6 FA accelerates fat accumulation and reduces lipid acid oxidation. Female mice were randomized and provided either a control-FA diet based on soy oil or a safflower oil diet rich in n6-FA at the time of mating (Fig 1A). All dams went through normal gestation and parturition, and litters were standardized to 7-8 pups per dam. All mating pairs, dams, and litters were housed in a temperature-controlled satellite facility maintained at 25°C. Gas Chromatography-Mass Spectrometry (GC-MS) analysis of plasma confirmed that n6-FA exposed litters (i.e., offspring of dams consuming diet rich in n6-FA) had significantly higher circulating levels of n6-FA, including arachidonic acid (20:4 n6), adrenic acid (22:4 n6), alongside reduced n3 fatty acids, including linolenic acid (18:3 n3), eicosatrienoic acid (20:3 n3), eicosapentaenoic acid (EPA 20:5 n3), docosapentaenoic acid(20:5 n6), and docosahexaenoic acid (DHA 22:6 n3; Table 1, Source Data File 2).

On PND12, body composition analysis by quantitative magnetic resonance (qMR) was assessed prior to pup sacrifice. Litters in the n6-FA exposure group had approximately 9% more body fat (p=0.029, n=15 litters/group) and a significantly greater fat-to-lean mass ratio (p=0.0322) than control-FA exposed pups, while no differences were observed in overall total body weight or lean mass (Fig 1B). Using indirect calorimetry with the environmental cabinet maintained at 25°C, PND12 litters in the n6-FA group had a significantly higher respiratory exchange ratio (RER, VCO_2/VO_2; p<0.0001, n=7-9 litters/group) compared to control-FA litters, both before and after suckling (Fig 1C). FAO calculated using the VO_2 and VCO_2 data in the post feeding window indicate reduced lipid oxidation in n6-FA litters (Fig 1D).

A separate cohort of n6-FA and control-FA litters were administered $^{13}C_{16}$-palmitate (100 mg/kg body weight) by gavage, placed into calorimetry cages, and whole-body FAO was used to quantify $^{13}CO_2$ emission by stable isotope gas exchange. The n6-FA exposed pups had significantly lower $^{13}CO_2$ vpdb emission, indicating diminished whole-body FAO (Fig 1E, p<0.001, n=4 litters/group). No differences were observed in blood glucose, triacylglycerides, or

insulin concentrations between groups, and $^{13}C_{16}$-palmitate uptake, quantified by GC/MS, into inguinal SAT, brown adipose tissue (BAT), liver, and muscle was equivalent (Suppl Fig 1A, B).

Omega-6 FA pups have less beige fat and reduced UCP1 levels.

We investigated the cellular morphology of inguinal SAT using H&E-stained sections. Consistent with our previous findings[36], n6-FA adipocytes were significantly larger than those from control pups (Fig 1F, $p<0.05$, n=6). Total TAG accumulation in the dissected inguinal SAT depot was significantly increased ($p=0.021$, n=3), consistent with the larger unilocular adipocytes and 9% increased body fat in the n6-FA pups (Fig 1G). No significant changes were observed in serum levels of key adipokines such as high molecular weight and total adiponectin, leptin, and retinol-binding protein 4 (RBP4) (Suppl Fig 1C).

Immunofluorescence for Perilipin1 (PLIN1), a coat protein for cytoplasmic lipid droplets within adipocytes, suggested that multilocular beige adipose tissue (BeAT) in inguinal SAT of n6-FA exposed pups was reduced (Fig 1H). Portions of adipose tissue having multilocular BeAT adipocyte regions, assessed by PLIN1 morphological inspection, were selected to quantify mitochondrial uncoupling protein 1 (UCP1), a marker of nutrient-oxidizing BeAT (Fig 2A). The distribution of UCP1 high staining overlapped with multilocular septa of beige adipocytes in inguinal SAT. Levels of UCP1 in multilocular adipocytes were significantly decreased within BeAT septa ($p=0.0008$, n=9/condition) in n6-SA SAT, followed by a trend of decreased UCP1 in the whole section ($p=0.052$), in the n6-FA sections. We confirmed the significant UCP1 decrease by immunoblotting, using the contralateral inguinal SAT from n6-FA and control-FA pups (Fig 2B, $p=0.027$, n=3/group). The ratio of mitochondrial superoxide dismutase 1 (SOD2) to mitochondrial import receptor subunit TOM20 in adipocytes is an indicator of mitochondrial dysfunction in obesity[54]. By PND12, inguinal SAT of n6-FA exposed pups had a significant increase in the SOD2/TOM20 ratio (Fig 2C, $p=0.047$, n=6/group), despite equivalent mitochondria amounts based on total TOM20 levels.

Isolated adipocytes of n6-FA SAT have diminished BeAT regulators.

We collected mature adipocytes from SVF preparations to assess protein levels and gene expression. The principal regulators of the nutrient-oxidizing adipocyte gene expression program, PPARγ and PPARγ coactivator 1 alpha (PGC1α)[55], were significantly decreased at the protein level in isolated adipocytes of the n6-FA exposed pups (Fig 2D, p=0.018 and 0.0007, respectively, n=4 individual litters/group). Moreover, critical transporters necessary for mitochondrial FAO, carnitine palmitoyl transferase 1A (CPT1A) and CPT1C, were also significantly decreased (p=0.002 and 0.013, respectively). Interestingly, the lower band for cytoplasmic lipid droplet protein PLIN1, which coordinates lipase access to the TAG droplet, was sharply increased in isolated adipocytes from n6-FA exposed pups (p=0.0007). The expression of genes necessary for nutrient-oxidation in beige adipocytes, Pgc1α, Ucp1, and Cell Death Inducing DFFA Like Effector A (Cidea), was notably decreased (p<0.05), while mRNA levels for PPARγ did not differ in isolated adipocytes from n6-rich pups (Fig 2E). Similar gene expression differences were observed in the whole inguinal adipose tissue (Suppl Fig 1D). Given these findings, we investigated whether *in vivo* n6-FA exposure alters the differentiation potential of ASCs by impacting the adipogenic regulators of BeAT.

Omega-6 FA program ASCs with decreased nutrient-oxidation and increased lipogenesis.

We isolated inguinal SAT ASCs for blood and endothelial lineage negative (CD45-, CD31-), mesenchymal stem cell positive (CD29+, CD34+), and adipocyte precursor positive (Sca1+) cells from n6-FA and control-FA exposed PND12 pups by fluorescence activated cell sorting from stromal vascular fraction (SVF) preparations[36]. ASCs were plated, allowed to adhere, and reach confluency, and then differentiated using standard adipogenic hormones, followed by six days in adipocyte maintenance media (Fig 3A). Differentiated adipocytes were stained using live-cell dyes for FAO (FAO blue), mitochondrial activity (TMRE), and triacylglyceride accumulation (LipidSpot). ASCs from the n6-FA exposed inguinal SAT that were differentiated

in vitro had significantly decreased FAO staining and mitochondrial activity (p=0.028 and 0.022, respectively), while overall lipid accumulation was not significantly changed (Fig 3B). Consistent with observations in isolated inguinal SAT adipocytes (Fig 2D and E), following *in vitro* differentiation of isolated ASCs, PPARγ, PGC1α, UCP1, and CPT1A protein levels were significantly decreased by in vivo n6-FA exposure (Fig 3C). Interestingly, no significant difference was observed for C/EBPα, which is needed for induction of PPARγ[56], and equivalent levels of FABP4 indicated both n6-FA and control ASCs differentiated into adipocytes. Given the sharp reduction in PPARγ and PGC1α protein levels in the n6-rich *in vitro* differentiated adipocytes, we measured gene expression for additional BeAT specific markers. In addition to significantly decreased Pparγ, Pgc1α, and Ucp1, we observed significantly lower expression of Cidea, Prdm16, Cox8b, and Cox7a1, in n6-FA ASCs following differentiation (Fig 3D). In contrast to the beige adipocyte program, the lipogenic markers, ATP-citrate lyase (Acly), Acetyl-CoA Carboxylase (Acc1), and Fatty Acid Synthase (Fasn) were significantly increased, as was expression of Adiponectin (AdipoQ), while Srebp2, the key player for cholesterol biosynthesis tended to increased expression (Fig 3D). Together, these findings suggest that *in vivo* n6-FA exposure programs the adipogenic potential of ASCs for nutrient storage, due to the less robust induction of beige adipocyte gene regulators.

ASCs programmed by n6-FA differentiate into less oxidative adipocytes.

Given the decreased FAO and mitochondrial activity measured by live cell stains, we investigated the cellular fuel preferences and oxidative capacities of ASCs isolated from inguinal SAT and differentiated *in vitro*. Adipocytes differentiated from n6-FA ASCs exhibited a marked reduction in FA fuel utilization when administered palmitate, as indicated by the energy map (Fig 4A, red arrow). A sizeable decrease in basal respiration, maximal respiration, ATP production coupled respiration, and spare respiratory capacity was observed in the *in vitro* differentiated adipocytes from n6-FA exposed ASCs, although non-mitochondrial respiration was same for

both groups (Fig 4B and C). Furthermore, when treated with mitochondrial FA transporter inhibitor etomoxir, which is used to demonstrate mitochondrial FAO specificity, *in vitro* differentiated adipocytes from n6-FA ASCs were less sensitive (Fig 4D, 20% compared to 55%), suggesting less reliance on FA as mitochondrial fuel. A similar oxygen consumption rate (OCR) profile occurred when glucose was the mitochondrial fuel substrate, with significant decreases basal respiration, and maximal respiration and spare respiratory capacity in the n6-FA group (Fig 4E and F). Addition of the pyruvate carrier inhibitor UK5099 indicated the n6-FA differentiated adipocytes were less sensitive to inhibiting pyruvate entry into mitochondrial oxidative phosphorylation (Fig 4G, 50% relative to 75%). No significant differences were observed when glutamine was the mitochondrial fuel substrate (Fig 4H-J). While nutrient-oxidizing adipocytes are specialized to uptake and oxidize both glucose and fatty acid, nutrient-storing adipocytes divert carbon away from respiration into nutrient storage pathways.

Omega-6 FA ASCs have low NR2F2 levels, giving rise to adipocytes with reduced mitochondrial ETC and FAO enzymes.

NR2F2 expression in metabolic tissues has been recognized since 2002[42]. Elegant work by Wang et al. demonstrated that the high-affinity ligand of NR2F2 is an atypical sphingolipid, 1-deoxysphingosine (1-DSO)[37]. We recently reported that NR2F2 is significantly decreased in PND12 pup ASCs following postnatal n6-FA exposure, and that 1-DSO treatment of undifferentiated immortalized ASCs increased beige adipocyte genes prior to differentiation[36]. This finding indicated that activated NR2F2 might alter ASC differentiation to a nutrient-oxidative differentiation trajectory. In isolated primary undifferentiated ASCs, NR2F2 protein was significantly reduced in pups exposed to n6-FA, and following *in vitro* adipocyte differentiation, NR2F2 levels declined equivalently (Fig 4K). In contrast to our previous finding, we differentiated ASCs isolated from control and n6-FA litters into adipocytes for proteomics analyses. Using the significant differentially expressed proteins (DEP), pathway enrichment

analysis identified decreased enzymes for lipid metabolism (LPL, PLIN1, ABHD5, SLC27A1), fatty acid oxidation (ACADS, ACSL1, SLC25A20), mitochondrial electron transport chain, and oxidative phosphorylation (ATP5F1A, UQCRC1. COX6C, ATP5MG), glucose metabolism (Mitochondrial Pyruvate Carrier1/2), and cholesterol biosynthesis in n6-FA adipocytes (Fig 4L, Source data file 1). Too few proteins were upregulated to return enriched pathways with an adjusted p-value less than 0.05 (Fig 4M).

Transient NR2F2 activation before differentiation enhanced FAO after differentiation.

Given that NR2F2 protein levels decline following in vitro differentiation, we reasoned that ligand activation of NR2F2 prior to differentiation would confer its function. We treated immortalized ASCs transiently with a 1-DSO pulse (300nM) flanking adipocyte differentiation induction, followed by maintenance media without 1-DSO for six days (Fig 5A). Activating NR2F2 in immortalized ASCs with transient 1-DSO enhanced the energetic profile and significantly increased basal, maximal OCR, and spare respiratory capacity compared to untreated controls (Fig 5B, C). Importantly, transient NR2F2 activation before adipocyte differentiation led to increased beige adipocyte regulators PPARγ, PGC1α and CPT1A after differentiation (Fig 5D). Using primary ASC isolated from n6-FA exposed pups, transient 1-DSO activation of NR2F2 (as in 5A) significantly restored the energetic profile, basal, and maximal FAO and spare respiratory capacity following *in vitro* differentiation into adipocytes (Fig 5E-G). In addition to enhancing FAO and regulators of beige adipogenesis, transient activation of NR2F2 led to persistent protein increases after differentiation for enzymes of mitochondrial ETC, oxidative phosphorylation, sphingolipid metabolism, ATP5 family of ATP synthases, and the NDUF family of mitochondrial Complex I components (Fig 5H, Source data file 1, proteomics, n=3, *pAdj*<0.05). Proteins that were significantly downregulated in response to the transient activation of NR2F2 in n6-FA ASCs included modulators of glucose metabolism, the TCA cycle, and lipid metabolism, including the de novo lipogenic enzymes ACLY, ACACA, ACACB, and

FASN (Fig 5I). Together, these findings indicate lasting changes to cellular metabolism resulting from transient NR2F2 activation prior to differentiation in the n6-FA ASCs, ultimately leading to broad changes in the mitochondrial enzymes and function.

NR2F2 ablation before differentiation phenocopies the n6-FA nutrient storing adipocytes. Rescue of the diminished FAO in n6-FA exposed pup ASCs by transient NR2F2 ligand activation suggests that NR2F2 operates upstream of, or parallel to, the beige differentiation program during adipogenesis. To test the loss of NR2F2 function and specificity of 1-DSO activation, we isolated ASCs from PND12 inguinal SAT (as above) using $NR2F2^{f/f}$ litters from the control-FA condition and deleted NR2F2 *in vitro* using Adeno-Cre (ΔNR2F2 ASCs) (Fig 6A). These ASCs grew and developed as wildtype ASCs under the *in vivo* control-FA exposure that produces BeAT, robust induction of BeAT regulators, and high levels of mitochondrial metabolism (Figures 2-4). After viral recovery and one passage of the ASCs, they were differentiated into adipocytes (as above), and differentiation potential, protein levels, and cellular metabolism were assessed. NR2F2 loss in ASCs resulted in significantly reduced FAO and mitochondrial activity by FAOBlue and TMRE live cell staining, while lipid droplet accumulation in adipocytes remained unchanged (Fig 6B). Importantly, immunoblotting confirmed that NR2F2 was efficiently deleted following Adeno-Cre transduction in ASCs, and following differentiation, that induction of BeAT regulator proteins, PGC1α and PPARγ, were reduced similarly to the n6-FA exposed inguinal ASCs (Fig 6C). *In vitro* deletion of NR2F2 also resulted in reduction of gene expression for Pparγ, Pgc1α, Cidea, Prdm16, Ucp1, and beige adipogenic regulator Ebf2 (Fig 6D). Deletion of NR2F2 prior to differentiation significantly reduced the OCR using palmitate as the fuel substrate, and transient treatment with 1-DSO failed to restore FAO (Fig 6E,F). These findings demonstrate the specificity of 1-DSO in activating NR2F2 in ASCs and support that NR2F2 is needed for FAO in the n6-FA adipocytes (Fig 5E-F).

We evaluated the activation status of the Wnt-CTNNb1 pathway using ASCs from the n6-FA and control-FA exposed pups for the known Wnt-Ctnnb1 responsive gene Axin2 [57]. In undifferentiated ASCs, Axin2 gene expression was significantly decreased, indicating that Wnt-CTNNb1 pathway was less active in n6-FA ASCs compared to the ASCs isolated from the control-FA pups. Continuous stimulation of the WNT/CTNNb1 signaling pathway in the 3T3L1 preadipocyte cell line led to chronic overexpression of NR2F2[38]. In alignment with the NR2F2 protein levels (Fig 4K), gene expression level of Nr2f2 was significantly decreased in the n6-FA ASCs, and mRNA for the Sptlc2 enzyme responsible for synthesizing 1-DSO was not significantly different (Fig 7A). Importantly, in n6-FA ASCs administered a selective CTNNb1 stabilizer to mimic WNT signal transduction activation of CTNNb1, the expression of Nr2f2, Sptlc2, and Axin2 were induced in ASCs isolated from the n6-FA exposed pups. Taken together, this indicates that CTNNb1 activation in primary ASCs induces Nr2f2 in the n6-FA exposed ASCs, linking WNT-CTNNb1 signal transduction to NR2F2 induction in primary ASCs.

DISCUSSION

Lipids transmitted from mother to infant provide energy dense nutrients, structural components, and potent signaling molecules for adipogenesis[58]. Over the first six months, infants significantly increase their body fat[59]. Early-life body fat accumulation serves dual roles, nutrient storage and oxidation, the latter of which is needed to defend core body temperature and supply energy needed for growth[60,61]. Both n6- and n3-FA are essential early in life for brain and eye development, but they also shape the development of the fat depots, possibly setting the stage for future obesity risk[62,63]. We investigated whole body and cellular energetics of PND12 pups using a model of excessive perinatal n6-FA exposure, at a point in life when metabolically active BeAT is highly abundant[64]. Litters exposed pre- and postnatally to a disproportionately high n6/n3 FA ratio during adipose development had a higher RER, reduced lipid oxidation

538 calculated by the equation 1.70 × VO_2 – 1.69 × VCO_2, and diminished whole-body FAO by
539 tracing ^{13}C-palmitate oxidation at 26°C (Fig 1C-E). The diminished FAO in litters occurred in the
540 face of equivalent palmitate levels present in both milk from dams (i.e., FA intake) and in
541 circulating plasma of the pups (Table1), suggesting that n6-FA exposed litters had sufficient
542 palmitate to oxidize but did not utilize it as a preferred fuel source. Analysis of the ^{13}C-palmitate
543 uptake indicated no differences for metabolic tissues, including BAT, liver, inguinal SAT, and
544 muscle (Supp Fig 1B). Together, these findings suggest that the high n6-FA exposure changed
545 the fuel utilization preference away from lipid oxidation, because the capacity to oxidize lipid as
546 a fuel source was blunted by exposure to high levels of n6-FA *in vivo*. A shift away from lipid
547 fuel preference is consistent with the metabolic programming we previously reported in the adult
548 setting, where pups exposed to a high n6/n3 FA ratio during the perinatal window, had
549 significantly higher RER and predisposition for adipose accumulation in adulthood[30].
550 This metabolic phenotype characterized by diminished whole-body FAO is, at least in
551 part, due to a defective metabolism within the SAT, given that n6-FA exposed SAT had a white
552 adipocyte morphology, size distribution, and 40% increase in stored triacylglycerides (Fig 1F-H).
553 The SAT morphology and lower whole-body FAO is consistent with the n6-FA pups having less
554 overall BeAT *in vivo.* The molecular signature of isolated adipocytes from PND12 n6-FA
555 exposed pups supports this observation, with less PGC1α, PPARγ, CPT1A, CPT1C, and UCP1,
556 which are key regulators of adipose mitochondrial FAO. PPARγ is necessary for both beige and
557 white adipogenesis, and zinc finger protein 423 (ZFP423) is thought to act as a molecular
558 "switch" between these two developmental programs[65]. In the beige program, EBF2 binds beige
559 gene promoters and recruits co-activators, which mediate decondensation of chromatin
560 structure and recruitment of PPARγ, promoting expression of beige loci and therefore beige
561 adipogenesis. In the white program, ZFP423 binds to EBF2, recruiting the NuRD corepressor
562 complex to block EBF2-dependent chromatin decondensation and subsequent PPARγ
563 recruitment, thereby promoting the nutrient storing white adipocyte program and not the nutrient

564 oxidizing beige one[65]. Conditional ablation of ZFP423 in inguinal white adipocytes increased
565 levels of Pgc1α, Prdm16, and Ucp1 expression, leading to a beige adipocyte morphology in the
566 presence of the potent PPARγ agonist rosiglitazone[65]. Intriguingly, NR2F2 has recently been
567 shown in a chicken model of adipogenesis to repress expression of ZFP423 by binding to sites
568 in the ZFP423 promoter, toggling to the beige adipocyte program[66]. In this study, we show that
569 NR2F2 levels are reduced in ASCs following perinatal exposure to high levels of n6-FA,
570 associating with a significant reduction of PGC1α, UCP1, and PPARγ *in vivo* (Fig 2), as well as
571 numerous beige genes (Fig 3) following *in vitro* differentiation. Taken together, our results
572 suggest a model for NR2F2 in which reduction of NR2F2 permits expression of ZFP423, which
573 in turn, blocks EBF2 function, promoting the white adipogenesis program. Consistent with our
574 current understanding of the beige and white adipogenesis is the loss of beige gene expression
575 and reciprocal induction of lipogenic genes, including Acly, Acc1, Fasn, and the principal
576 regulator of the cholesterol biosynthesis pathway, Srebf2 (Fig 3).
577 In alignment with the diminished whole-body FAO observed by ^{13}C-palmitate tracing
578 was the marked decrease in cellular FAO of *in vitro* differentiated ASCs isolated from the n6-FA
579 exposed pups (Fig 4). When provided palmitate as the fuel source, adipocytes differentiated *in*
580 *vitro* had a 50% reduction in basal, maximal, and ATP-coupled respiration, with less sensitivity
581 to the mitochondrial FA uptake inhibitor etomoxir. Interestingly, when glucose was provided as
582 the cellular metabolic fuel substrate, both basal and maximal respiration rates were also
583 reduced, while minimal differences were observed with glutamine (Fig 4). Together, this finding
584 suggests a fundamental difference in the oxidative phosphorylation capacity of adipocyte
585 mitochondria following a high n6-FA perinatal exposure. The pathway enrichment analyses of
586 the proteome from *in vitro* differentiated ASCs supports this notion, in that, downregulation of
587 OXPHOS and ETC proteins ATP5F1A, ATP5MG, ACOX, ACADS, COX6C, and UQCRC1 was
588 observed (Fig 4).This indicates a significant difference in the key enzymes responsible for
589 mitochondrial oxidation and energy production, which is a well-documented characteristic of

mitochondrial dysfunction of adipocytes in obesity[67,68], which is established as early as PND12 in mice. The observations of impaired *in vitro* palmitate and glucose substrate oxidation, the loss of beige adipocyte regulator levels (Fig 3), and 40% more triacylglyceride in the PND12 fat pad (Fig 1), is consistent with adipogenic programming that is prone to store nutrients rather than oxidize them.

We identified previously that NR2F2 was reduced in isolated inguinal fat pad ASCs from n6-FA exposed pups, alongside an altered mitochondrial gene expression profile[36]. We extend those findings to show that ligand activation of NR2F2 in ASCs leads to persistent formation of nutrient oxidizing adipocytes. NR2F2 is expressed during development and is critical for energy homeostasis and adipocyte biology[39-43]. As a nuclear receptor type 2 family member, NR2F2 can bind DNA directly, as well as dimerize with other nuclear receptors to either activate or repress transcription, depending on the cellular context[69]. While NR2F2 is known as a metabolic regulator, defining the mechanisms of NR2F2 function *in vivo* has remained a challenge. There is conflicting evidence of NR2F2 function during adipogenesis[39-44]. Genomic loss of Nr2f2 is embryonic lethal in mice[70], and the genomic heterozygous mice are viable but smaller in size than WT littermates[71], have more skeletal muscle, less white AT, and greater bone formation[39,40]. Paradoxically, the genomic Nr2f2 heterozygous adult mice had greater energy expenditure, glucose clearance, and resistance to diet-induced obesity, thought to be due to the imbalance of metabolic tissues [39,40,42,69,71].

Metabolically active adipocytes are established by known regulatory factors, most prominently PPARγ, PGC1α, and PRDM16, which cooperate to implement mitochondrial gene expression as part of the beige adipocyte metabolic program[55,72]. Here, the perinatal n6-FA exposure led to isolated ASCs with significantly lower NR2F2 protein levels (Fig 4K). We found that transient NR2F2 activation in ASCs led to persistent increases of metabolic activators PPARγ, PGC1α, and CPT1A, along with partially restoring the diminished FAO capacity due to perinatal n6-FA programming (Fig 5). Although NR2F2 activation with 1-DSO was transient, the

whole cell proteome revealed installation of lasting increases in mitochondrial complex I, oxidative phosphorylation, and electron transport chain components (Fig5 H, I).

The increase in mitochondrial complex components supporting FAO corresponded to decreases in proteins for glycolysis, TCA cycle, *de novo* fatty acid synthesis, and curiously, some enzymes for FAO and fatty acid transport. In other words, NR2F2 activation increased levels of some enzymes responsible for FAO, while simultaneously decreasing enzymes involved in the same process. Perhaps this dual effect resulted in adipocyte mitochondria with an increased ability to handle fatty acids nearly as effectively as adipocytes differentiated from control ASCs. Importantly, 1-DSO treatment is specific to NR2F2 activation in ASCs, because transient treatment failed to boost FAO following *in vitro* ablation of NR2F2 (Fig 6). Instead, ASCs isolated from NR2F2$^{f/f}$ pups, which developed normally as wildtype ASCs under the control-FA perinatal exposure, accumulated lipid droplets equivalently to AdCon-transduced control ASCs, but lacked robust induction of Pparγ, Pgc1α, Cidea, Prdm16, and Ucp1 beige genes when NR2F2 was knocked down. Altogether, ASC-specific decreases of NR2F2 that occur during perinatal n6-FA exposure coincided with diminished FAO, which could be partially restored by activating NR2F2 with ligand 1-DSO in the undifferentiated state.

It remains unclear what regulates the levels of NR2F2 mRNA and protein in ASCs from our model of perinatal FA exposures. In the 3T3-L1 preadipocyte cell line, chronic WNT3a-stimulated activation of CTNNb1 in undifferentiated cells and throughout 10-days of adipocyte differentiation, induced and sustained NR2F2 levels in adipocytes, suppressing adipogenesis via modifications of chromatin architecture[38]. Because NR2F2 normally decreases during adipocyte differentiation (Fig4K), sustaining its levels throughout differentiation may have influenced those findings. Despite the evidence that CTNNb1 activation opposes adipogenesis, key effectors of WNT signaling (CTNNb1 and TCF7L2) are expressed in mature adipocytes, and disrupting them leads to adipocyte hypertrophy, inflammation, glucose intolerance, and insulin resistance[73-75]. Recent findings highlight the potential of "WNT positive ASCs" in

promoting beige adipocyte formation and recruitment, and when transplanted, WNT positive ASCs enhanced glucose metabolism in recipients[76]. We previously reported that ASCs from n6-FA pups expressed an mRNA signature consistent with inhibited CTNNb1, including downregulated Wingless-type MMTV integration site 6 and 9a (Wnt6 and Wnt9a), its receptor Frizzled 1 (Fzd1), and signal transducer Akt1, which have been shown to activate CTNNb1 [76]. Conversely, n6-FA exposed ASCs had upregulated secreted Frizzled Related Protein 2 and 4 (Sfrp2 and Sfrp4), which have been shown to antagonize the WNT/CTNNb1 signaling pathway[77].

Interestingly, n3-FA supplementation has been shown to increase Wnt/CTNNb1 levels and signaling *in vitro* and in animal models. For example, pregnant female rats that were induced to have preeclampsia had increased Wnt and b-catenin protein levels in their brain tissue when they were supplemented with n3-FA using both eicosapentaenoic and docosahexaenoic acids blended at 4:1[78]. In another study, supplementation of docosahexaenoic acid in doses above 10mM increased WNT/CTNNb1 signaling in human iPSC-derived neuronal progenitor cells *in vitro* in the presence of Wnt ligand (Wnt3a)[79]. In our study, ASCs from n6-FA exposed pups had significantly downregulated Axin2, a known CTNNb1 target gene. Stimulation of n6-FA ASCs with a selective CTNNb1 stabilizer significantly increased Axin2, which coincided with induced gene expression of Nr2f2 and Sptlc2, an enzyme responsible for synthesizing 1-DSO[37], the endogenous ligand for NR2F2 (Fig 7A). Upregulation of Nr2f2 mRNA following CTNNb1 activation in the n6-FA primary ASCs is consistent with NR2F2 being downstream of WNT/CTNNb1 gene regulation.

Cumulatively, our findings support a model in which ASCs exposed to a high n6- relative to n3-FA ratio tapers WNT mediated activation of CTNNb1, leading to reduced induction of NR2F2 and less robust expression of beige regulators PPARγ, PGC1α, Cidea, Prdm16, and Ucp1. These ASCs, when differentiated, give rise to mature adipocytes with diminished electron transport chain and oxidative phosphorylation protein components, blunted nutrient oxidation,

while retaining enhanced triacylglyceride accumulation (Fig 7B). Our findings suggest that, from as early as PND12 in mice, inguinal SAT may be programmed for nutrient storing white adipocytes, potentially leading to an obesity-prone phenotype that persists into adulthood, possibly via epigenetic regulation[30].

LIMITATIONS AND FUTURE RESEARCH

This study differed from our previous studies of early-life FA exposures and SAT development [30,36], in that maternal dietary FA composition was based on extremely n6-FA rich safflower oil. Although dams and sires were provided the safflower oil diet at the time of pairing, thereby confining the FA exposure within the perinatal setting, we cannot exclude the possibility of germline effects[80]. Moreover, this dietary FA composition is not representative of the US maternal dietary n6- relative to n3-FA ratio, which has escalated dramatically over the decades due to an overload of n6-FA[11], reaching an n6/n3 ratio between 20:1 and 40:1[81]. Because dietary oil sources, such as corn, soybean, sunflower oils, are typically high in n6-FA, an important issue will be to lower maternal consumption of n6-FA containing sources while increasing dietary sources containing n3-FA, such as flax and fish oils[62]. The current study did not investigate the classes of signaling lipids, which are enzymatic products of both n6- and n3-FA. For example, our group recently identified 12,13-diHOME, an oxylipin derivative of linoleic acid (18:2 n6) that is inversely related to infant fat mass at 1-month of age[82]. Interestingly, NR2F2 activating ligand 1-DSO was not detected in either the dam's milk or pup's plasma by lipid mass spectrometry, suggesting that it is synthesized as an intracellular ligand or acts as a localized paracrine signaling lipid. To that end, it would be important to evaluate the intracellular signaling lipids, including the NR2F2 ligand 1-DSO, within ASCs isolated from n6-FA and control-FA exposures, for differences in lipids influencing adipogenic potential. Critically, NR2F2 binds CTNNb1[83], suggesting that direct CTNNb1-NR2F2 interaction may play a key role in modulating how ASCs respond during adipogenesis early in life. Although we suggest that

NR2F2 acts upstream of the beige regulator genetic program, it is unclear whether NR2F2 is upstream of, or acting in parallel to, these other important regulators. Future work will focus on defining the sequential timing of NR2F2 action and any ASC-specific NR2F2 interacting proteins that might differ between control and n6-FA perinatal exposures.

CONCLUSION

Obesity, defined by excessive white adipose tissue accumulation, is a complex gene-nutrient-lifestyle interaction disease, with roots in early-life development. The metabolic regulator NR2F2 plays a key role in establishing adipocytes with the capacity to oxidize nutrients, at least in the mouse pup. While still somewhat controversial in humans, activating beige adipocytes in rodents offsets metabolic dysfunction associated with diet-induced obesity. Understanding mechanisms governing how metabolically active adipogenesis is established, especially in response to dietary bioactive FA and their signaling lipid derivatives, could pave the way for promising interventions that protect against childhood obesity.

ACKNOWLEDGEMENT

We would like to thank the Flow cytometry core at The University of Oklahoma health Sciences center (OUHSC). We are also thankful to the Flow cytometry core at Oklahoma Medical Research Foundation for assistance with Aurora Spectral Flow Cytometry (Grant number: 1S10OD028479-01). This work is supported by grants: R24GM137786 (IDeA National Resource for Quantitative Proteomics) and P20GM103447 (Oklahoma INBRE) to MK, NIH (HL 156856, HL 137799) and AHA (TPA97002) to PRN, and Oklahoma Center for Adult Stem Cell Research (OCASCR) and the Presbyterian Health Foundation Equipment Grant to MCR.

AUTHOR CONTRIBUTION

Conceptualization- MCR, SD. **Methodology-**SD, RV, GPM, AEM, JWF, MK. **Investigation-** MCR, SD, RV, GPM. **Data Curation-** SD, RV, AEM, GPM, GKD, KH, MK, JWF. **Formal analysis-** MCR, SD, RV, JWF, MK. **Resources**- MCR, PRN. **Writing-Original Draft-** SD, MCR, GPM, RV. **Writing-Review and Editing**- MCR, GPM, RV, PRN. **Visualization**- MCR. **Supervision**- MCR. **Funding acquisition**- MCR.

ETHICS DECLARATIONS

Competing Interests

The authors declare no competing interests.

INCLUSION AND DIVERSITY

One or more of the authors of this paper self-identifies as an underrepresented ethnic minority in their field of research.

Figure legends

Figure 1. High n6 exposure alters fat mass percentage, RER, and adipocyte cellularity. (A) Diagram of experimental design. (B) Body composition of control and high n6-FA exposed pups at Postnatal day 12 (PND12). Each data point is the mean mass, lean body mass, fat mass, ratio of fat to lean mass, or fat mass percentage of one litter of pups at PND12 (n=13-15 litters). (C) Indirect calorimetry of control and high n6-exposed litters. Dams were removed for the 2h pre- and 3h post-nursing periods to measure the Respiratory Exchange Ratio (VCO2/VO2: Scale 0.5-1.0) of pups in a litter. Data are presented as means ± SEM (n=7-9). (D) Fatty acid oxidation (FAO) calculated using the equation ($1.70 \times VO_2 - 1.69 \times VCO_2$) (n=7-9). (E) Pups were administered $^{13}C_{16}$-palmitate (100 mg/kg body weight) and the litters placed into cages in an Indirect Calorimeter cabinet held at 25°C to quantify $^{13}CO_2$ stable isotope gas exchange as a measure of whole-body FAO (n=3 per group). (F) H&E staining of control and n6-FA exposed pup SAT (inguinal fat) and quantification of cellularity (n=7-8). Scale bar is 100 μm. (G) Quantification of SAT triglyceride (TAG) levels (n=5). (H) Immunofluorescence staining of inguinal adipose tissue with anti-PLIN1 antibody (green) and DAPI (blue) (n=5 neonatal inguinal SAT sections from independent litters per control/n6-FA group). The scale bar is 100 μm. Data are expressed as mean ± SEM, statistical significance is denoted by *p < 0.05, **p < 0.01, ***p < 0.001, ****p < 0.0001 by t-test.

Figure 2. Expression of beige adipocyte proteins in SAT and adipocytes. (A) Immunofluorescence staining of inguinal SAT from PND12 mice with anti-UCP1 (red) and anti-PLIN1 (green) antibodies. Nuclei (blue) were stained with DAPI. Morphologically defined white and beige regions were quantified separately for UCP1 staining, which was significantly decreased in n6-FA group (n=8-11 neonatal SAT section from independent litters per control/n6 group). (B, C) Analysis of UCP1, SOD2, and TOM20 in inguinal fat pads through Western blotting. CypA was used as the reference protein to normalize loading (n=3-6 neonatal SAT tissue from independent litters per control/n6-FA group). (D, E) Levels of key adipocyte proteins and mRNA were measured through Western blotting and qPCR in mature adipocytes isolated from inguinal fat from control and n6-FA pups. (n=3-4 pooled adipocytes from neonatal SAT tissue from independent litters per control/n6-FA group). Data are expressed as mean ± SEM, statistical significance is denoted by *p < 0.05, **p < 0.01, ***p < 0.001, ****p < 0.0001 by t-test.

Figure 3. High n6-FA exposure reduces expression of beige markers while upregulating lipogenic markers in adipocytes generated from them. (A) Experimental design. (B) Differentiated beige adipocytes were stained with LipidSpot (green; lipid droplets), TMRE (red; mitochondria), and FAOBlue (blue; fatty acid oxidation). n=3 wells containing ASCs isolated from inguinal SAT from independent litters per control/n6-FA group. Intensity of LipidSpot, TMRE, and FAOBlue staining was quantified using image J software (n=6. Two images per well). Scale bar 100 μM. (C, D) Protein levels and mRNA expression in differentiated adipocytes were quantified through semiquantitative Western blots and qPCR (n=3 wells containing ASCs isolated from inguinal SAT from independent litters per control/n6-FA group). Data are expressed as mean ± SEM, statistical significance is denoted by *p < 0.05, **p < 0.01, ***p < 0.001, ****p < 0.0001 by one-way ANOVA and Tukey's correction.

Figure 4. High n6-FA exposure in ASCs inhibits fatty acid oxidation in adipocytes. ASCs were isolated from control and n6-FA exposed pups, plated, and differentiated to beige adipocytes, which were used for metabolic assays in Fig A-J (n=5-7 ASC pools from independent litters per control/n6-FA group). (A) Energy map of control and high n6-FA exposed adipocytes when palmitate was supplied as fuel. (B) Kinetic graphs for oxygen consumption rate (OCR) and extracellular acidification rate (ECAR). (C) OCR for basal, maximal, ATP production-coupled respiration, and spare respiratory capacity in differentiated adipocytes. (D) Sensitivity to Etomoxir during maximal respiration (E, F) Energy map, OCR for basal, maximal, ATP production-coupled respiration, and spare respiratory capacity when glucose was supplied as fuel source. (G) Sensitivity to UK5099 during maximal respiration (H, I) Energy map, OCR for basal, maximal, ATP production-coupled respiration, and spare respiratory capacity when glutamine was supplied as fuel source. (J) Sensitivity to BPTES during maximal respiration (K) Analysis of NR2F2 protein levels in undifferentiated and differentiated beige adipocytes derived from flow-sorted ASCs from control and n6-FA pups through. (L, M) Proteomics data from differentiated beige adipocytes derived from control and n6-FA primary ASCs, followed by pathway enrichment analyses. (n=3 wells containing differentiated ASCs isolated from inguinal SAT from independent litters per control/n6-FA group for all the experiments; K-M). Data are expressed as mean ± SEM, statistical significance is denoted by *p < 0.05, **p < 0.01, ***p < 0.001, ****p < 0.0001 by multiple comparison t-test for B, one-way ANOVA for F, I, K, and t-test for the rest.

Figure 5. Transient NR2F2 activation in n6-FA ASCs improves fatty acid oxidation and alters mitochondrial proteins in adipocytes. (A) Experimental design. Immortalized adipocyte precursor cells (APCs) were differentiated to beige adipocytes ± a 4-day pulse treatment with 1-DSO in the early phase of differentiation, as shown in the schematic. Following differentiation, cells were assayed for metabolic activity and protein abundance (n=3-7 wells containing immortalized ASCs for Con and 1-DSO; Fig A-D). (B, C) Energy map, basal, maximal respiration and spare respiratory capacity in control and 1-DSO treated beige adipocytes when palmitate was used as the fuel source. (D) Treatment with NR2F2 ligand 1-DSO increased expression of beige markers in beige adipocytes differentiated from APCs evaluated through Western blotting. (E-G) OCR kinetic graph, energy map, basal, maximal respiration and spare respiratory capacity in beige differentiated ASCs (± 1-DSO during differentiation as in panel A) isolated from control and n6-FA pups, when palmitate was supplied as fuel source (n=5-11 wells per group). (H, I) Proteomics data from beige differentiated ASCs (± 1-DSO during differentiation as in panel A) isolated from n6-FA pups, followed by pathway enrichment analyses, showing important metabolic pathways were altered significantly between groups (n=3 wells per group). Data are expressed as mean ± SEM, statistical significance is denoted by *p < 0.05, **p < 0.01, ***p < 0.001, ****p < 0.0001 by one-way ANOVA for C, G, multiple comparison t-test for E and t-test for the rest.

Figure 6. Ablation of NR2F2 *in vitro* suppresses expression of beige proteins following differentiation. (A) Diagram of experimental design. ASCs were isolated from $Nr2f2^{f/f}$ pups, plated, treated with Adeno-Cre (AdCre) or control adenovirus (AdCon) to ablate NR2F2, followed by differentiation into beige adipocytes. Following differentiation, cells were assayed for adipogenic markers. (B) Differentiated adipocytes were stained with LipidSpot (green; lipid

droplets), TMRE (red; mitochondria), and FAOBlue (blue; fatty acid oxidation) and quantified in Image J (n=4 wells containing ASCs isolated from inguinal SAT from independent litters). (C, D) Protein and mRNA levels of NR2F2 and other key regulators were quantified in ASCs ± *in vitro* ablation of NR2F2 through Western blotting and qPCR (n=3 wells per group). (E, F) Basal, maximal respiration, and OCR (kinetic graph) of beige differentiated ASCs (n=6-8 wells per group). Data are expressed as mean ± SEM, statistical significance is denoted by *p < 0.05, **p < 0.01 by t-test for B and one-way ANOVA for the rest.

Figure 7. (A) mRNA expression of Nr2f2, Axin2, and Sptlc2 in ASCs ± Wnt agonist 1(48h) quantified through qPCR (n=3 wells per group). (B) Model showing effects of excess n6-FA exposure on ASCs and how that affects adipocyte metabolism. ASCs exposed to n6-FA ratio have a diminished WNT mediated activation of CTNNb1 gene signature, leading to poor induction of NR2F2 and lower expression of beige regulators PPARγ, PGC1α, Cidea, and Prdm16. These ASCs differentiate, give rise to mature adipocytes with diminished electron transport chain and oxidative phosphorylation protein components, blunted nutrient oxidation, while retaining an enhanced capacity for triacylglyceride accumulation. Data are expressed as mean ± SEM, statistical significance is denoted by *p < 0.05, **p < 0.01, ***p < 0.001, ****p < 0.0001 by one-way ANOVA.

879 **Table 1**

	Mom Milk (pmoles/mg protein)					Pup Plasma (pmoles/ul)				
	Con		n6		p value	Con		n6		p value
Fatty Acids	Mean	SD	Mean	SD		Mean	SD	Mean	SD	
8:0	849	474	645	407	0.4272	298	94	932	550	**0.0365**
10:0	23110	10816	26672	17680	0.6659	274	188	88	41	0.0605
12:0	15825	7195	13706	6962	0.6020	470	231	326	111	0.2092
14:0	14030	5274	13224	6902	0.8160	1111	317	725	224	**0.0373**
16:0	22821	7801	20184	7905	0.5585	586	118	462	149	0.1435
16:1 n-7	5352	1910	2867	1260	**0.0250**	377	81	184	105	**0.0057**
18:0	3503	1262	2940	1198	0.4300	111	22	109	10	0.8985
18:1	32363	14477	21442	12794	0.1827	2002	277	1552	615	0.1470
18:2 n-6	6789	2103	12556	5713	**0.0387**	703	122	809	207	0.3111
18:3 n-6	222	96	400	203	**0.0697**	29	6	37	15	0.2633
18:3 n-3	2181	684	181	108	**0.0007**	205	65	87	78	**0.0180**
20:1 n-6	2344	835	1411	597	**0.0487**	61	36	30	30	0.1390
20:2 n-6	1850	591	2863	1125	0.0672	75	38	85	39	0.6484
20:3 n-6	1037	381	1353	531	0.2391	104	22	104	33	0.9905
20:4 n-6	858	336	1385	552	0.0609	520	84	670	117	**0.0309**
20:3 n-3	230	70	12	5	**0.0006**	30	6	18	6	**0.0048**
20:5 n-3	121	42	7	3	**0.0011**	45	8	17	18	**0.0105**
22:4 n-6	319	129	547	221	**0.0437**	29	6	49	16	**0.0269**
22:5 n-6	63	24	205	79	**0.0026**	56	8	115	41	**0.0162**
22:3 n-3	5	1	0	0	**0.0004**	5	0	5	0	0.1645
22:5 n-3	177	65	12	6	**0.0015**	42	6	21	16	**0.0234**
22:6 n-3	180	59	40	19	**0.0015**	231	35	124	79	**0.0200**
MCFA	53815	22519	54246	31430	0.9776	2153	692	2070	502	0.8178
SatFA	80138	29945	77370	39853	0.8891	2850	798	2642	630	0.6277
MUFA	40060	16982	25721	14478	0.1357	2453	312	1766	745	0.0772
PUFA	14032	4446	19561	8363	0.1623	2107	281	2142	449	0.8767
LC-PUFA	4839	1647	6424	2483	0.1987	1169	136	1209	229	0.7234
n-6 PUFA	11138	3598	19308	8235	**0.0433**	1542	202	1870	415	0.1236
n-3 PUFA	2894	895	252	140	**0.0007**	565	83	272	197	**0.0129**
n6/n3	3.84	0.44	81.15	14.55	**0.0000**	2.74	0.12	9.12	4.49	**0.0176**
AA/(EPA+DHA)	2.76	0.37	30.44	5.88	**0.0000**	1.87	0.10	6.23	3.08	**0.0178**
SatFA/MUFA	2.13	0.55	3.54	2.61	0.2075	1.16	0.24	1.62	0.45	0.0589
SatFA/(MUFA+PUFA)	1.54	0.33	1.85	1.12	0.5041	0.62	0.12	0.69	0.10	0.2811

18:1/18:0	8.96	2.28	7.11	2.30	0.1740	18.73	4.69	14.04	5.11	0.1292
16:1/16:0	0.23	0.02	0.15	0.05	**0.0034**	0.65	0.14	0.38	0.11	**0.0043**
20:4n-6/20:3n-6	0.82	0.05	1.02	0.10	**0.0010**	4.82	1.10	6.68	1.07	**0.0137**
18:3n-6/18:2n-6	0.03	0.01	0.03	0.01	0.8243	0.04	0.01	0.04	0.01	0.7065
Total FA	134230	49489	122651	57761	0.7045	7365	1310	6550	1710	0.3776

Table 1: GC-MS analyses of mother's milk and plasma from the pups for quantifying levels of omega-3 (n3) and omega-6 (n6) fatty acids (n=5-7).

REFERENCES

1. Lister, N.B., Baur, L.A., Felix, J.F., Hill, A.J., Marcus, C., Reinehr, T., Summerbell, C., and Wabitsch, M. (2023). Child and adolescent obesity. Nat Rev Dis Primers *9*, 24. 10.1038/s41572-023-00435-4.
2. Ward, Z.J., Long, M.W., Resch, S.C., Giles, C.M., Cradock, A.L., and Gortmaker, S.L. (2017). Simulation of Growth Trajectories of Childhood Obesity into Adulthood. N Engl J Med *377*, 2145-2153. 10.1056/NEJMoa1703860.
3. Heymsfield, S.B., and Wadden, T.A. (2017). Mechanisms, Pathophysiology, and Management of Obesity. N Engl J Med *376*, 1492. 10.1056/NEJMc1701944.
4. O'Connor, E.A., Evans, C.V., Burda, B.U., Walsh, E.S., Eder, M., and Lozano, P. (2017). Screening for Obesity and Intervention for Weight Management in Children and Adolescents: Evidence Report and Systematic Review for the US Preventive Services Task Force. JAMA *317*, 2427-2444. 10.1001/jama.2017.0332.
5. Rankin, J., Matthews, L., Cobley, S., Han, A., Sanders, R., Wiltshire, H.D., and Baker, J.S. (2016). Psychological consequences of childhood obesity: psychiatric comorbidity and prevention. Adolesc Health Med Ther *7*, 125-146. 10.2147/AHMT.S101631.
6. Widdowson, E.M., and McCance, R.A. (1975). A review: new thoughts on growth. Pediatric research *9*, 154-156. 10.1203/00006450-197503000-00010.
7. Rasmussen, K.M. (2001). The "fetal origins" hypothesis: challenges and opportunities for maternal and child nutrition. Annu Rev Nutr *21*, 73-95. 10.1146/annurev.nutr.21.1.73.
8. Friedman, J.E. (2018). Developmental Programming of Obesity and Diabetes in Mouse, Monkey, and Man in 2018: Where Are We Headed? Diabetes *67*, 2137-2151. 10.2337/dbi17-0011.
9. Koletzko, B., Brands, B., Grote, V., Kirchberg, F.F., Prell, C., Rzehak, P., Uhl, O., Weber, M., and Early Nutrition Programming, P. (2017). Long-Term Health Impact of Early Nutrition: The Power of Programming. Ann Nutr Metab *70*, 161-169. 10.1159/000477781.
10. Wesolowski, S.R., El Kasmi, K.C., Jonscher, K.R., and Friedman, J.E. (2017). Developmental origins of NAFLD: a womb with a clue. Nature Reviews Gastroenterology & Hepatology *14*, 81-96. 10.1038/nrgastro.2016.160.
11. Muhlhausler, B.S., and Ailhaud, G.P. (2013). Omega-6 polyunsaturated fatty acids and the early origins of obesity. Curr Opin Endocrinol Diabetes Obes *20*, 56-61. 10.1097/MED.0b013e32835c1ba7.
12. Massiera, F., Barbry, P., Guesnet, P., Joly, A., Luquet, S., Moreilhon-Brest, C., Mohsen-Kanson, T., Amri, E.Z., and Ailhaud, G. (2010). A Western-like fat diet is sufficient to induce a gradual enhancement in fat mass over generations. J Lipid Res *51*, 2352-2361. 10.1194/jlr.M006866.
13. Ailhaud, G., Guesnet, P., and Cunnane, S.C. (2008). An emerging risk factor for obesity: does disequilibrium of polyunsaturated fatty acid metabolism contribute to excessive adipose tissue development? Br J Nutr *100*, 461-470. 10.1017/S0007114508911569.
14. Ailhaud, G., Massiera, F., Weill, P., Legrand, P., Alessandri, J.M., and Guesnet, P. (2006). Temporal changes in dietary fats: role of n-6 polyunsaturated fatty acids in excessive adipose tissue development and relationship to obesity. Prog Lipid Res *45*, 203-236. 10.1016/j.plipres.2006.01.003.
15. Donahue, S.M., Rifas-Shiman, S.L., Gold, D.R., Jouni, Z.E., Gillman, M.W., and Oken, E. (2011). Prenatal fatty acid status and child adiposity at age 3 y: results from a US pregnancy cohort. Am J Clin Nutr *93*, 780-788. 10.3945/ajcn.110.005801.
16. Novak, E.M., and Innis, S.M. (2011). Impact of maternal dietary n-3 and n-6 fatty acids on milk medium-chain fatty acids and the implications for neonatal liver metabolism. Am J Physiol Endocrinol Metab *301*, E807-817. 10.1152/ajpendo.00225.2011.

17. Pedersen, L., Lauritzen, L., Brasholt, M., Buhl, T., and Bisgaard, H. (2012). Polyunsaturated fatty acid content of mother's milk is associated with childhood body composition. Pediatr Res *72*, 631-636. 10.1038/pr.2012.127.
18. Moon, R.J., Harvey, N.C., Robinson, S.M., Ntani, G., Davies, J.H., Inskip, H.M., Godfrey, K.M., Dennison, E.M., Calder, P.C., Cooper, C., and Group, S.W.S.S. (2013). Maternal plasma polyunsaturated fatty acid status in late pregnancy is associated with offspring body composition in childhood. J Clin Endocrinol Metab *98*, 299-307. 10.1210/jc.2012-2482.
19. Young, B.E., Levek, C., Reynolds, R.M., Rudolph, M.C., MacLean, P., Hernandez, T.L., Friedman, J.E., and Krebs, N.F. (2018). Bioactive components in human milk are differentially associated with rates of lean and fat mass deposition in infants of mothers with normal vs. elevated BMI. Pediatr Obes. 10.1111/ijpo.12394.
20. Rudolph, M.C., Young, B.E., Lemas, D.J., Palmer, C.E., Hernandez, T.L., Barbour, L.A., Friedman, J.E., Krebs, N.F., and MacLean, P.S. (2016). Early infant adipose deposition is positively associated with the n-6 to n-3 fatty acid ratio in human milk independent of maternal BMI. Int J Obes (Lond). 10.1038/ijo.2016.211.
21. de Vries, P.S., Gielen, M., Rizopoulos, D., Rump, P., Godschalk, R., Hornstra, G., and Zeegers, M.P. (2014). Association between polyunsaturated fatty acid concentrations in maternal plasma phospholipids during pregnancy and offspring adiposity at age 7: the MEFAB cohort. Prostaglandins Leukot Essent Fatty Acids *91*, 81-85. 10.1016/j.plefa.2014.04.002.
22. Massiera, F., Saint-Marc, P., Seydoux, J., Murata, T., Kobayashi, T., Narumiya, S., Guesnet, P., Amri, E.Z., Negrel, R., and Ailhaud, G. (2003). Arachidonic acid and prostacyclin signaling promote adipose tissue development: a human health concern? J Lipid Res *44*, 271-279. 10.1194/jlr.M200346-JLR200.
23. Korotkova, M., Gabrielsson, B., Lonn, M., Hanson, L.A., and Strandvik, B. (2002). Leptin levels in rat offspring are modified by the ratio of linoleic to alpha-linolenic acid in the maternal diet. J Lipid Res *43*, 1743-1749.
24. Korotkova, M., Gabrielsson, B.G., Holmang, A., Larsson, B.M., Hanson, L.A., and Strandvik, B. (2005). Gender-related long-term effects in adult rats by perinatal dietary ratio of n-6/n-3 fatty acids. Am J Physiol Regul Integr Comp Physiol *288*, R575-579. 10.1152/ajpregu.00342.2004.
25. Rudolph, M.C., Young, B.E., Jackson, K.H., Krebs, N.F., Harris, W.S., and MacLean, P.S. (2016). Human Milk Fatty Acid Composition: Comparison of Novel Dried Milk Spot Versus Standard Liquid Extraction Methods. J Mammary Gland Biol Neoplasia. 10.1007/s10911-016-9365-4.
26. Kahn, C.R., Wang, G., and Lee, K.Y. (2019). Altered adipose tissue and adipocyte function in the pathogenesis of metabolic syndrome. J Clin Invest *129*, 3990-4000. 10.1172/JCI129187.
27. Symonds, M.E., Pope, M., Sharkey, D., and Budge, H. (2012). Adipose tissue and fetal programming. Diabetologia *55*, 1597-1606. 10.1007/s00125-012-2505-5.
28. Desoye, G., and Herrera, E. (2021). Adipose tissue development and lipid metabolism in the human fetus: The 2020 perspective focusing on maternal diabetes and obesity. Prog Lipid Res *81*. ARTN 101082 10.1016/j.plipres.2020.101082.
29. Puche-Juarez, M., Toledano, J.M., Ochoa, J.J., Diaz-Castro, J., and Moreno-Fernandez, J. (2023). Influence of Adipose Tissue on Early Metabolic Programming: Conditioning Factors and Early Screening. Diagnostics *13*. ARTN 1510 10.3390/diagnostics13091510.
30. Rudolph, M.C., Jackman, M.R., Presby, D.M., Houck, J.A., Webb, P.G., Johnson, G.C., Soderborg, T.K., de la Houssaye, B.A., Yang, I.V., Friedman, J.E., and MacLean, P.S.

(2018). Low Neonatal Plasma n-6/n-3 PUFA Ratios Regulate Offspring Adipogenic Potential and Condition Adult Obesity Resistance. Diabetes *67*, 651-661. 10.2337/db17-0890.

31. Berry, R., and Rodeheffer, M.S. (2013). Characterization of the adipocyte cellular lineage in vivo. Nat Cell Biol *15*, 302-308. 10.1038/ncb2696.
32. Berry, R., Jeffery, E., and Rodeheffer, M.S. (2014). Weighing in on adipocyte precursors. Cell Metab *19*, 8-20. 10.1016/j.cmet.2013.10.003.
33. Church, C.D., Berry, R., and Rodeheffer, M.S. (2014). Isolation and study of adipocyte precursors. Methods Enzymol *537*, 31-46. 10.1016/B978-0-12-411619-1.00003-3.
34. Jeffery, E., Church, C.D., Holtrup, B., Colman, L., and Rodeheffer, M.S. (2015). Rapid depot-specific activation of adipocyte precursor cells at the onset of obesity. Nat Cell Biol *17*, 376-385. 10.1038/ncb3122.
35. Jeffery, E., Wing, A., Holtrup, B., Sebo, Z., Kaplan, J.L., Saavedra-Pena, R., Church, C.D., Colman, L., Berry, R., and Rodeheffer, M.S. (2016). The Adipose Tissue Microenvironment Regulates Depot-Specific Adipogenesis in Obesity. Cell Metab *24*, 142-150. 10.1016/j.cmet.2016.05.012.
36. Varshney, R., Das, S., Trahan, G.D., Farriester, J.W., Mullen, G.P., Kyere-Davies, G., Presby, D.M., Houck, J.A., Webb, P.G., Dzieciatkowska, M., et al. (2023). Neonatal intake of Omega-3 fatty acids enhances lipid oxidation in adipocyte precursors. iScience *26*, 105750. 10.1016/j.isci.2022.105750.
37. Wang, T., Wang, Z., de Fabritus, L., Tao, J., Saied, E.M., Lee, H.J., Ramazanov, B.R., Jackson, B., Burkhardt, D., Parker, M., et al. (2021). 1-deoxysphingolipids bind to COUP-TF to modulate lymphatic and cardiac cell development. Dev Cell *56*, 3128-3145 e3115. 10.1016/j.devcel.2021.10.018.
38. Okamura, M., Kudo, H., Wakabayashi, K., Tanaka, T., Nonaka, A., Uchida, A., Tsutsumi, S., Sakakibara, I., Naito, M., Osborne, T.F., et al. (2009). COUP-TFII acts downstream of Wnt/beta-catenin signal to silence PPARgamma gene expression and repress adipogenesis. Proc Natl Acad Sci U S A *106*, 5819-5824. 10.1073/pnas.0901676106.
39. Xie, X., Qin, J., Lin, S.H., Tsai, S.Y., and Tsai, M.J. (2011). Nuclear receptor chicken ovalbumin upstream promoter-transcription factor II (COUP-TFII) modulates mesenchymal cell commitment and differentiation. Proc Natl Acad Sci U S A *108*, 14843-14848. 10.1073/pnas.1110236108.
40. Li, L., Xie, X., Qin, J., Jeha, G.S., Saha, P.K., Yan, J., Haueter, C.M., Chan, L., Tsai, S.Y., and Tsai, M.J. (2009). The nuclear orphan receptor COUP-TFII plays an essential role in adipogenesis, glucose homeostasis, and energy metabolism. Cell Metab *9*, 77-87. 10.1016/j.cmet.2008.12.002.
41. Jeong, B.C., Kang, I.H., Hwang, Y.C., Kim, S.H., and Koh, J.T. (2014). MicroRNA-194 reciprocally stimulates osteogenesis and inhibits adipogenesis via regulating COUP-TFII expression. Cell Death Dis *5*, e1532. 10.1038/cddis.2014.485.
42. Ashraf, U.M., Sanchez, E.R., and Kumarasamy, S. (2019). COUP-TFII revisited: Its role in metabolic gene regulation. Steroids *141*, 63-69. 10.1016/j.steroids.2018.11.013.
43. Scholtes, C., and Giguere, V. (2022). Transcriptional control of energy metabolism by nuclear receptors. Nat Rev Mol Cell Biol. 10.1038/s41580-022-00486-7.
44. Zhang, P., Bennoun, M., Gogard, C., Bossard, P., Leclerc, I., Kahn, A., and Vasseur-Cognet, M. (2002). Expression of COUP-TFII in metabolic tissues during development. Mech Dev *119*, 109-114. 10.1016/s0925-4773(02)00286-1.
45. Planchais, J., Boutant, M., Fauveau, V., Qing, L.D., Sabra-Makke, L., Bossard, P., Vasseur-Cognet, M., and Pegorier, J.P. (2015). The role of chicken ovalbumin upstream promoter transcription factor II in the regulation of hepatic fatty acid oxidation and gluconeogenesis in newborn mice. Am J Physiol Endocrinol Metab *308*, E868-878. 10.1152/ajpendo.00433.2014.

46. Robinson, C.E., Wu, X., Nawaz, Z., Onate, S.A., and Gimble, J.M. (1999). A corepressor and chicken ovalbumin upstream promoter transcriptional factor proteins modulate peroxisome proliferator-activated receptor-gamma2/retinoid X receptor alpha-activated transcription from the murine lipoprotein lipase promoter. Endocrinology *140*, 1586-1593. 10.1210/endo.140.4.6653.
47. Galarraga, M., Campion, J., Munoz-Barrutia, A., Boque, N., Moreno, H., Martinez, J.A., Milagro, F., and Ortiz-de-Solorzano, C. (2012). Adiposoft: automated software for the analysis of white adipose tissue cellularity in histological sections. J Lipid Res *53*, 2791-2796. 10.1194/jlr.D023788.
48. Schneider, C.A., Rasband, W.S., and Eliceiri, K.W. (2012). NIH Image to ImageJ: 25 years of image analysis. Nat Methods *9*, 671-675. 10.1038/nmeth.2089.
49. Schindelin, J., Arganda-Carreras, I., Frise, E., Kaynig, V., Longair, M., Pietzsch, T., Preibisch, S., Rueden, C., Saalfeld, S., Schmid, B., et al. (2012). Fiji: an open-source platform for biological-image analysis. Nat Methods *9*, 676-682. 10.1038/nmeth.2019.
50. Hong, G., Fan, S., Phyu, T., Maheshwari, P., Hoppe, M.M., Phuong, H.M., de Mel, S., Poon, M., Ng, S.B., and Jeyasekharan, A.D. (2019). Multiplexed Fluorescent Immunohistochemical Staining, Imaging, and Analysis in Histological Samples of Lymphoma. J Vis Exp. 10.3791/58711.
51. Im, K., Mareninov, S., Diaz, M.F.P., and Yong, W.H. (2019). An Introduction to Performing Immunofluorescence Staining. Methods Mol Biol *1897*, 299-311. 10.1007/978-1-4939-8935-5_26.
52. Rudolph, M.C., Wellberg, E.A., Lewis, A.S., Terrell, K.L., Merz, A.L., Maluf, N.K., Serkova, N.J., and Anderson, S.M. (2014). Thyroid hormone responsive protein Spot14 enhances catalysis of fatty acid synthase in lactating mammary epithelium. J Lipid Res *55*, 1052-1065. 10.1194/jlr.M044487.
53. Rudolph, M.C., Karl Maluf, N., Wellberg, E.A., Johnson, C.A., Murphy, R.C., and Anderson, S.M. (2012). Mammalian fatty acid synthase activity from crude tissue lysates tracing (1)(3)C-labeled substrates using gas chromatography-mass spectrometry. Anal Biochem *428*, 158-166. 10.1016/j.ab.2012.06.013.
54. Han, Y.H., Buffolo, M., Pires, K.M., Pei, S., Scherer, P.E., and Boudina, S. (2016). Adipocyte-Specific Deletion of Manganese Superoxide Dismutase Protects From Diet-Induced Obesity Through Increased Mitochondrial Uncoupling and Biogenesis. Diabetes *65*, 2639-2651. 10.2337/db16-0283.
55. Cheng, L., Wang, J., Dai, H., Duan, Y., An, Y., Shi, L., Lv, Y., Li, H., Wang, C., Ma, Q., et al. (2021). Brown and beige adipose tissue: a novel therapeutic strategy for obesity and type 2 diabetes mellitus. Adipocyte *10*, 48-65. 10.1080/21623945.2020.1870060.
56. Wu, Z., Rosen, E.D., Brun, R., Hauser, S., Adelmant, G., Troy, A.E., McKeon, C., Darlington, G.J., and Spiegelman, B.M. (1999). Cross-regulation of C/EBP alpha and PPAR gamma controls the transcriptional pathway of adipogenesis and insulin sensitivity. Mol Cell *3*, 151-158. 10.1016/s1097-2765(00)80306-8.
57. Jho, E.H., Zhang, T., Domon, C., Joo, C.K., Freund, J.N., and Costantini, F. (2002). Wnt/beta-catenin/Tcf signaling induces the transcription of Axin2, a negative regulator of the signaling pathway. Mol Cell Biol *22*, 1172-1183. 10.1128/MCB.22.4.1172-1183.2002.
58. Bobinski, R., and Bobinska, J. (2020). Fatty acids of human milk - a review. Int J Vitam Nutr Res, 1-12. 10.1024/0300-9831/a000651.
59. Fields, D.A., Gilchrist, J.M., Catalano, P.M., Gianni, M.L., Roggero, P.M., and Mosca, F. (2011). Longitudinal body composition data in exclusively breast-fed infants: a multicenter study. Obesity (Silver Spring) *19*, 1887-1891. 10.1038/oby.2011.11.
60. Kuzawa, C.W. (1998). Adipose tissue in human infancy and childhood: an evolutionary perspective. Am J Phys Anthropol *Suppl 27*, 177-209. 10.1002/(sici)1096-8644(1998)107:27+<177::aid-ajpa7>3.0.co;2-b.

61. Roberts, S.B., and Young, V.R. (1988). Energy costs of fat and protein deposition in the human infant. The American journal of clinical nutrition *48*, 951-955. 10.1093/ajcn/48.4.951.
62. Simopoulos, A.P. (2016). An Increase in the Omega-6/Omega-3 Fatty Acid Ratio Increases the Risk for Obesity. Nutrients *8*, 128. 10.3390/nu8030128.
63. Mennitti, L.V., Oliveira, J.L., Morais, C.A., Estadella, D., Oyama, L.M., do Nascimento, C.M., and Pisani, L.P. (2015). Type of fatty acids in maternal diets during pregnancy and/or lactation and metabolic consequences of the offspring. J Nutr Biochem *26*, 99-111. 10.1016/j.jnutbio.2014.10.001.
64. Bruder, J., and Fromme, T. (2022). Global Adipose Tissue Remodeling During the First Month of Postnatal Life in Mice. Front Endocrinol (Lausanne) *13*, 849877. 10.3389/fendo.2022.849877.
65. Shao, M., Zhang, Q., Truong, A., Shan, B., Vishvanath, L., Li, L., Seale, P., and Gupta, R.K. (2021). ZFP423 controls EBF2 coactivator recruitment and PPARgamma occupancy to determine the thermogenic plasticity of adipocytes. Genes Dev *35*, 1461-1474. 10.1101/gad.348780.121.
66. Li, X., Sun, D., Wang, Z., Zhao, Q., Liu, Y., and Hou, Z. (2024). Transcriptional regulatory mechanism of NR2F2 and ZNF423 in avian preadipocyte differentiation. Gene *897*, 148106. 10.1016/j.gene.2023.148106.
67. Song, H., Zhang, X., Wang, J., Wu, Y., Xiong, T., Shen, J., Lin, R., Xiao, T., and Lin, W. (2023). The regulatory role of adipocyte mitochondrial homeostasis in metabolism-related diseases. Front Physiol *14*, 1261204. 10.3389/fphys.2023.1261204.
68. Das, S., Mukhuty, A., Mullen, G.P., and Rudolph, M.C. (2024). Adipocyte Mitochondria: Deciphering Energetic Functions across Fat Depots in Obesity and Type 2 Diabetes. Int J Mol Sci *25*. 10.3390/ijms25126681.
69. Polvani, S., Pepe, S., Milani, S., and Galli, A. (2019). COUP-TFII in Health and Disease. Cells *9*. 10.3390/cells9010101.
70. Pereira, F.A., Qiu, Y., Zhou, G., Tsai, M.J., and Tsai, S.Y. (1999). The orphan nuclear receptor COUP-TFII is required for angiogenesis and heart development. Genes Dev *13*, 1037-1049.
71. Lin, F.J., Qin, J., Tang, K., Tsai, S.Y., and Tsai, M.J. (2011). Coup d'Etat: an orphan takes control. Endocr Rev *32*, 404-421. 10.1210/er.2010-0021.
72. Inagaki, T., Sakai, J., and Kajimura, S. (2017). Transcriptional and epigenetic control of brown and beige adipose cell fate and function. Nat Rev Mol Cell Biol *18*, 527. 10.1038/nrm.2017.72.
73. Chen, M., Lu, P., Ma, Q., Cao, Y., Chen, N., Li, W., Zhao, S., Chen, B., Shi, J., Sun, Y., et al. (2020). CTNNB1/beta-catenin dysfunction contributes to adiposity by regulating the cross-talk of mature adipocytes and preadipocytes. Sci Adv *6*, eaax9605. 10.1126/sciadv.aax9605.
74. Bagchi, D.P., Li, Z., Corsa, C.A., Hardij, J., Mori, H., Learman, B.S., Lewis, K.T., Schill, R.L., Romanelli, S.M., and MacDougald, O.A. (2020). Wntless regulates lipogenic gene expression in adipocytes and protects against diet-induced metabolic dysfunction. Mol Metab *39*, 100992. 10.1016/j.molmet.2020.100992.
75. Chen, X., Ayala, I., Shannon, C., Fourcaudot, M., Acharya, N.K., Jenkinson, C.P., Heikkinen, S., and Norton, L. (2018). The Diabetes Gene and Wnt Pathway Effector TCF7L2 Regulates Adipocyte Development and Function. Diabetes *67*, 554-568. 10.2337/db17-0318.
76. Liu, Z., Chen, T., Zhang, S., Yang, T., Gong, Y., Deng, H.W., Bai, D., Tian, W., and Chen, Y. (2022). Discovery and functional assessment of a novel adipocyte population driven by intracellular Wnt/beta-catenin signaling in mammals. Elife *11*. 10.7554/eLife.77740.

77. Park, J.R., Jung, J.W., Lee, Y.S., and Kang, K.S. (2008). The roles of Wnt antagonists Dkk1 and sFRP4 during adipogenesis of human adipose tissue-derived mesenchymal stem cells. Cell Prolif *41*, 859-874. 10.1111/j.1365-2184.2008.00565.x.
78. ShamsEldeen, A.M., Mehesen, M.N., Aboulhoda, B.E., Rashed, L.A., Elsebaie, M.M., Mohamed, E.A., and Gamal, M.M. (2021). Prenatal intake of omega-3 promotes Wnt/beta-catenin signaling pathway, and preserves integrity of the blood-brain barrier in preeclamptic rats. Physiol Rep *9*, e14925. 10.14814/phy2.14925.
79. Zhao, W.N., Hylton, N.K., Wang, J., Chindavong, P.S., Alural, B., Kurtser, I., Subramanian, A., Mazitschek, R., Perlis, R.H., and Haggarty, S.J. (2019). Activation of WNT and CREB signaling pathways in human neuronal cells in response to the Omega-3 fatty acid docosahexaenoic acid (DHA). Mol Cell Neurosci *99*, 103386. 10.1016/j.mcn.2019.06.006.
80. de la Rocha, C., Rodriguez-Rios, D., Ramirez-Chavez, E., Molina-Torres, J., de Jesus Flores-Sierra, J., Orozco-Castellanos, L.M., Galvan-Chia, J.P., Sanchez, A.V., Zaina, S., and Lund, G. (2022). Cumulative Metabolic and Epigenetic Effects of Paternal and/or Maternal Supplementation with Arachidonic Acid across Three Consecutive Generations in Mice. Cells *11*. 10.3390/cells11061057.
81. Mariamenatu, A.H., and Abdu, E.M. (2021). Overconsumption of Omega-6 Polyunsaturated Fatty Acids (PUFAs) versus Deficiency of Omega-3 PUFAs in Modern-Day Diets: The Disturbing Factor for Their "Balanced Antagonistic Metabolic Functions" in the Human Body. J Lipids *2021*, 8848161. 10.1155/2021/8848161.
82. Wolfs, D., Lynes, M.D., Tseng, Y.H., Pierce, S., Bussberg, V., Darkwah, A., Tolstikov, V., Narain, N.R., Rudolph, M.C., Kiebish, M.A., et al. (2021). Brown Fat-Activating Lipokine 12,13-diHOME in Human Milk Is Associated With Infant Adiposity. J Clin Endocrinol Metab *106*, e943-e956. 10.1210/clinem/dgaa799.
83. Yan, X., Qu, X., Liu, B., Zhao, Y., Xu, L., Yu, S., Wang, J., Wang, L., and Su, J. (2021). Autophagy-Induced HDAC6 Activity During Hypoxia Regulates Mitochondrial Energy Metabolism Through the beta-Catenin/COUP-TFII Axis in Hepatocellular Carcinoma Cells. Front Oncol *11*, 742460. 10.3389/fonc.2021.742460.

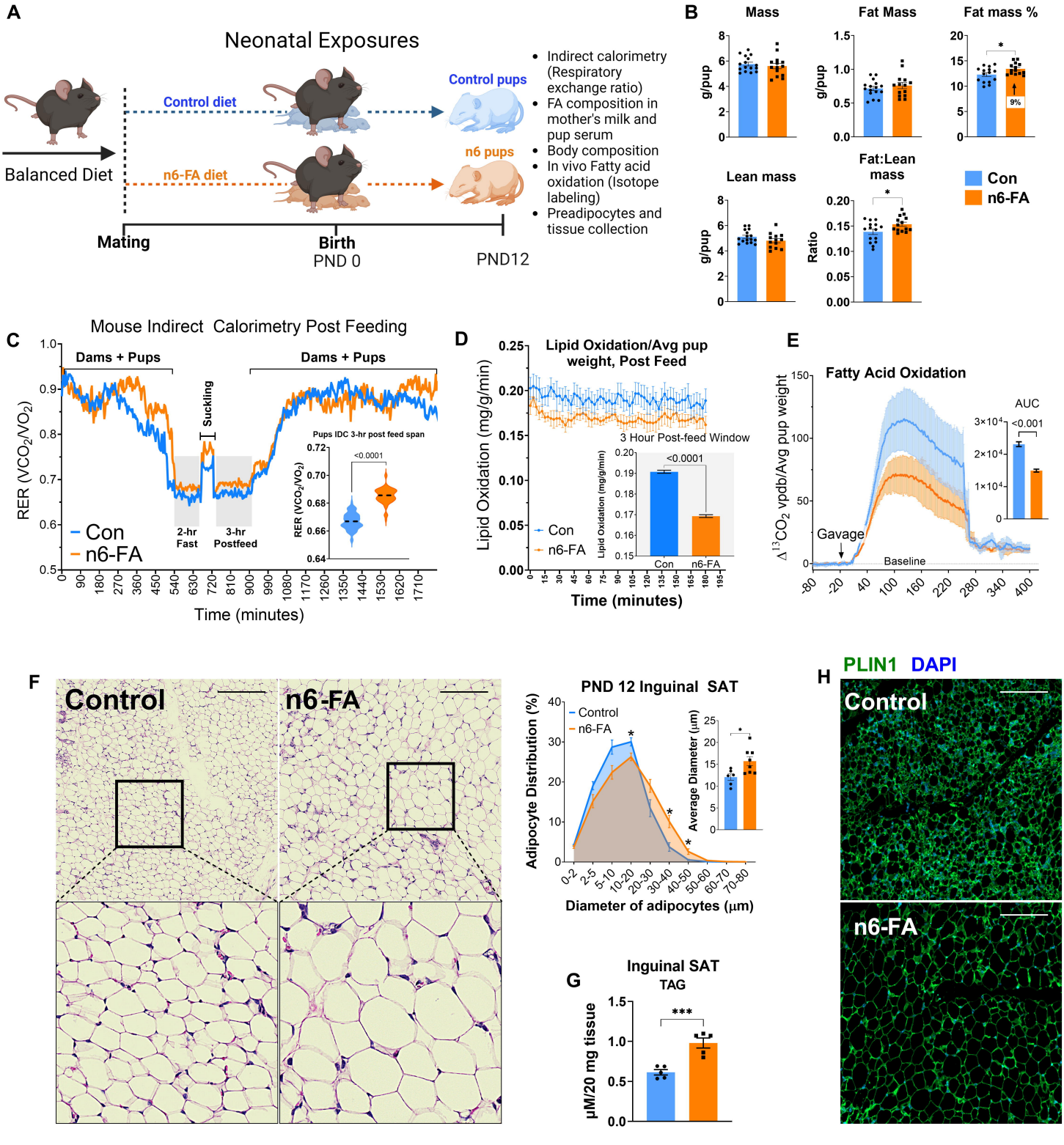
A
Neonatal Exposures
Balanced Diet
Control diet
n6-FA diet
Control pups
n6 pups
Mating
Birth
PND 0
PND12
Indirect calorimetry (Respiratory exchange ratio)
FA composition in mother's milk and pup serum
Body composition
In vivo Fatty acid oxidation (Isotope labeling)
Preadipocytes and tissue collection
B
Mass
Fat Mass
Fat mass %
Lean mass
Fat:Lean mass
g/pup
Ratio
9%
Con
n6-FA
C
Mouse Indirect Calorimetry Post Feeding
Dams + Pups
Suckling
2-hr Fast
3-hr Postfeed
RER (VCO2/VO2)
Time (minutes)
Pups IDC 3-hr post feed span
<0.0001
D
Lipid Oxidation/Avg pup weight, Post Feed
Lipid Oxidation (mg/g/min)
3 Hour Post-feed Window
Time (minutes)
E
Fatty Acid Oxidation
Δ13CO2 vpdb/Avg pup weight
Gavage
Baseline
AUC
F
Control
n6-FA
PND 12 Inguinal SAT
Adipocyte Distribution (%)
Average Diameter (μm)
Diameter of adipocytes (μm)
G
Inguinal SAT
TAG
μM/20 mg tissue
***
H
PLIN1 DAPI
Control
n6-FA

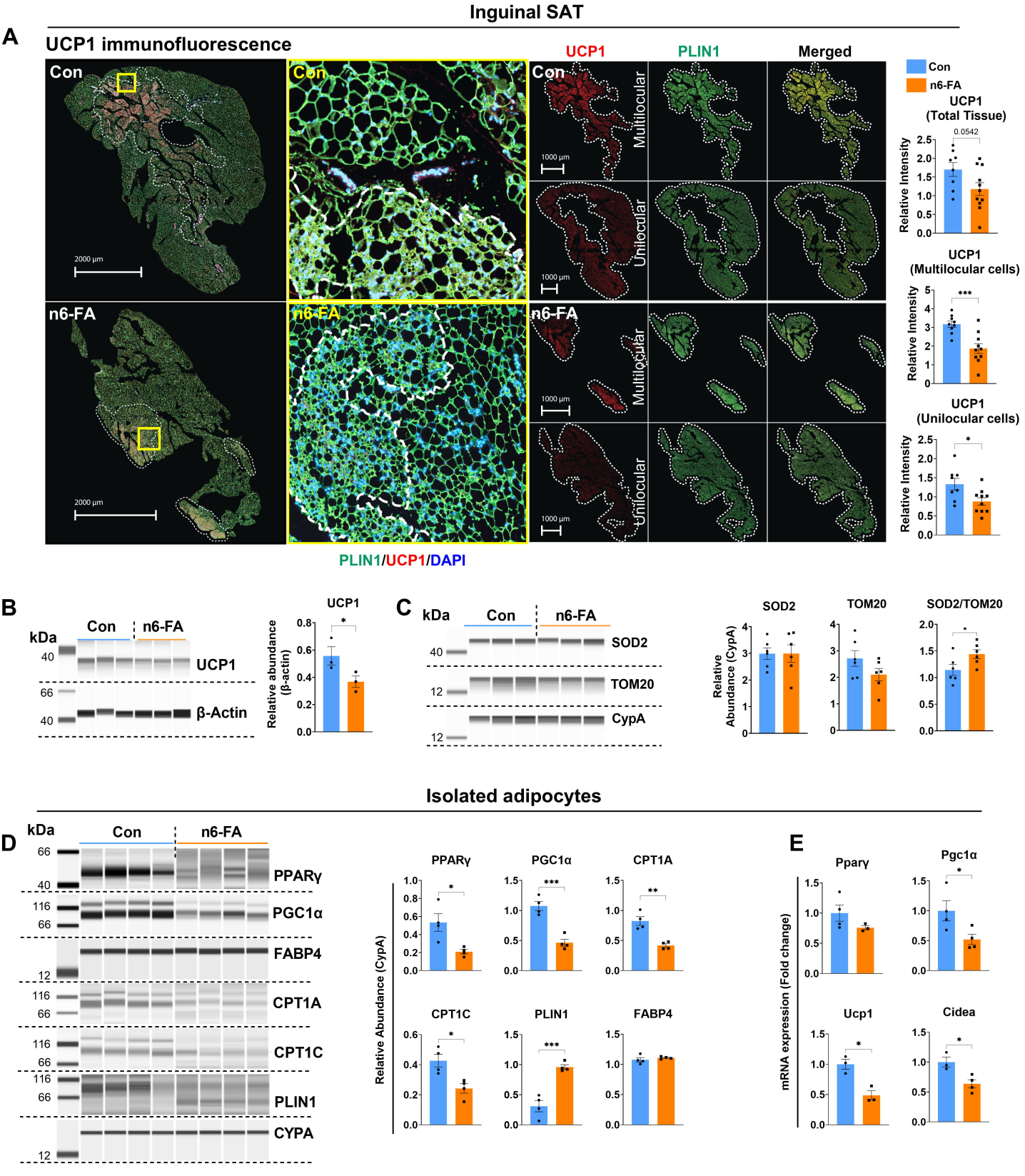
Inguinal SAT
A
UCP1 immunofluorescence
Con
n6-FA
2000 μm
UCP1
PLIN1
Merged
Multilocular
Unilocular
1000 μm
PLIN1/UCP1/DAPI
Con
n6-FA
UCP1 (Total Tissue)
0.0542
UCP1 (Multilocular cells)
***
UCP1 (Unilocular cells)
*
Relative Intensity
B
kDa
40
UCP1
66
40
β-Actin
Relative abundance (β-actin)
C
SOD2
12
TOM20
CypA
Relative Abundance (CypA)
SOD2
TOM20
SOD2/TOM20
Isolated adipocytes
D
66
40
PPARγ
116
66
PGC1α
FABP4
12
CPT1A
CPT1C
PLIN1
CYPA
PPARγ
PGC1α
CPT1A
CPT1C
PLIN1
FABP4
E
Pparγ
Pgc1α
Ucp1
Cidea
mRNA expression (Fold change)

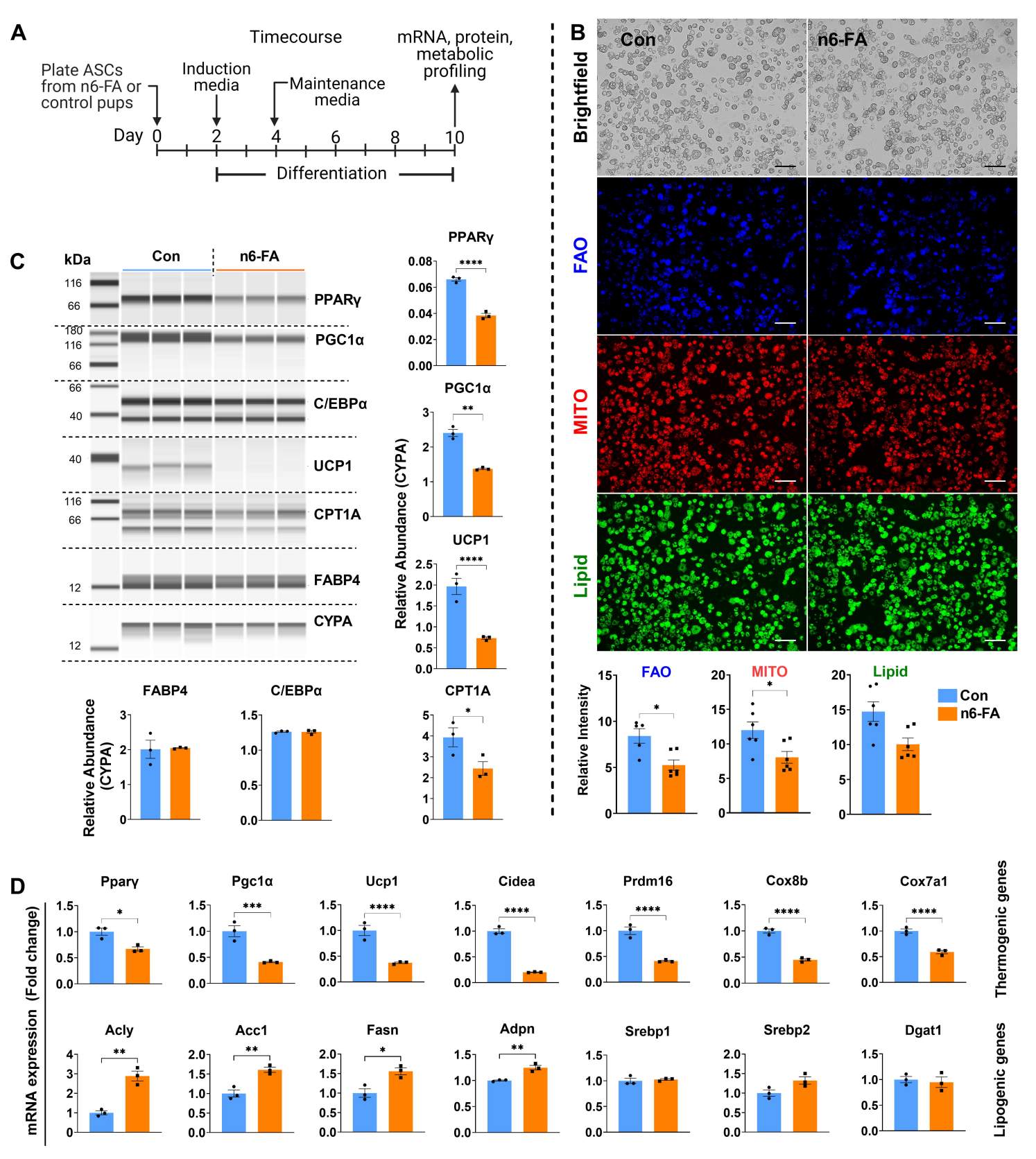
A
Timecourse
mRNA, protein, metabolic profiling
Plate ASCs from n6-FA or control pups
Induction media
Maintenance media
Day 0 2 4 6 8 10
Differentiation
B
Con
n6-FA
Brightfield
FAO
MITO
Lipid
FAO
MITO
Lipid
Relative Intensity
Con
n6-FA
C
kDa
Con
n6-FA
116
66
PPARγ
180
116
66
PGC1α
66
40
C/EBPα
40
UCP1
116
66
CPT1A
12
FABP4
12
CYPA
PPARγ
PGC1α
UCP1
Relative Abundance (CYPA)
FABP4
C/EBPα
CPT1A
Relative Abundance (CYPA)
D
mRNA expression (Fold change)
Pparγ
Pgc1α
Ucp1
Cidea
Prdm16
Cox8b
Cox7a1
Thermogenic genes
Acly
Acc1
Fasn
Adpn
Srebp1
Srebp2
Dgat1
Lipogenic genes

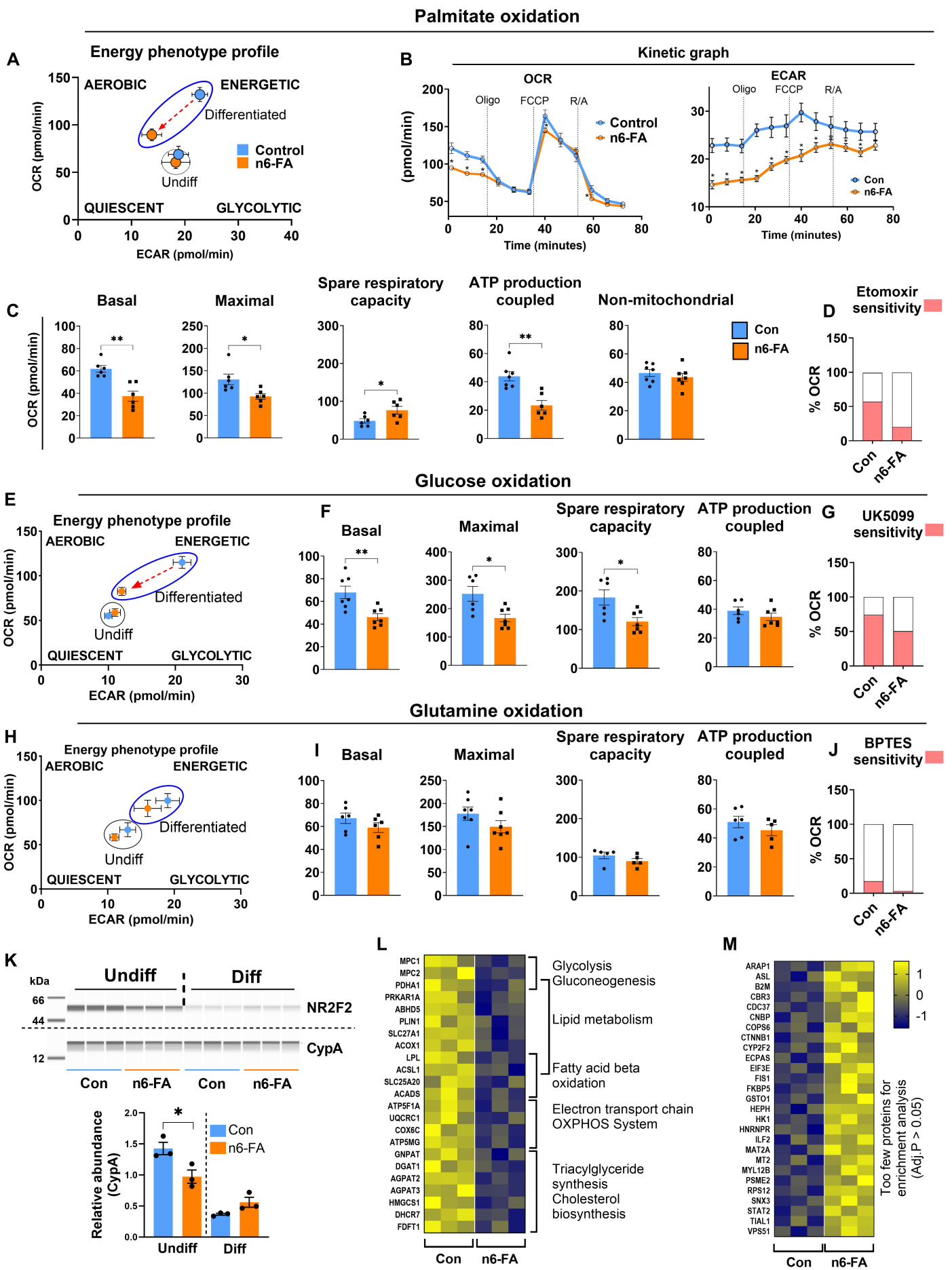
Palmitate oxidation
A
Energy phenotype profile
AEROBIC
ENERGETIC
Differentiated
Undiff
Control
n6-FA
QUIESCENT
GLYCOLYTIC
OCR (pmol/min)
ECAR (pmol/min)
B
Kinetic graph
OCR
ECAR
Oligo
FCCP
R/A
Control
n6-FA
Con
Time (minutes)
C
Basal
Maximal
Spare respiratory capacity
ATP production coupled
Non-mitochondrial
OCR (pmol/min)
D
Etomoxir sensitivity
% OCR
Glucose oxidation
E
F
G
UK5099 sensitivity
Glutamine oxidation
H
I
J
BPTES sensitivity
K
kDa
Undiff
Diff
66
44
12
NR2F2
CypA
Relative abundance (CypA)
L
MPC1
MPC2
PDHA1
PRKAR1A
ABHD5
PLIN1
SLC27A1
ACOX1
LPL
ACSL1
SLC25A20
ACADS
ATP5F1A
UQCRC1
COX6C
ATP5MG
GNPAT
DGAT1
AGPAT2
AGPAT3
HMGCS1
DHCR7
FDFT1
Glycolysis
Gluconeogenesis
Lipid metabolism
Fatty acid beta oxidation
Electron transport chain OXPHOS System
Triacylglyceride synthesis
Cholesterol biosynthesis
M
ARAP1
ASL
B2M
CBR3
CDC37
CNBP
COPS6
CTNNB1
CYP2F2
ECPAS
EIF3E
FIS1
FKBP5
GSTO1
HEPH
HK1
HNRNPR
ILF2
MAT2A
MT2
MYL12B
PSME2
RPS12
SNX3
STAT2
TIAL1
VPS51
Too few proteins for enrichment analysis (Adj.P > 0.05)

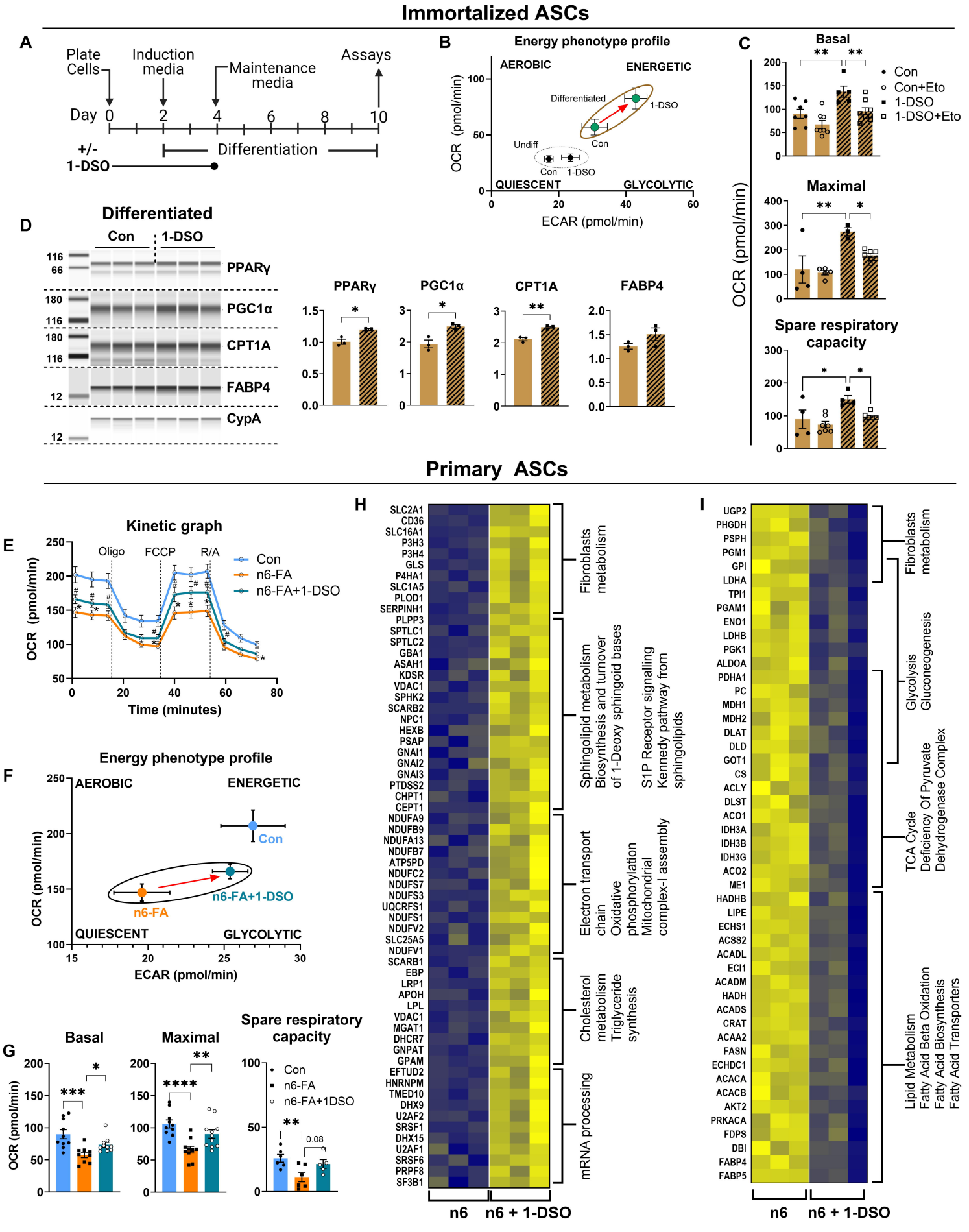
Immortalized ASCs
A
Plate Cells
Induction media
Maintenance media
Assays
Day 0 2 4 6 8 10
+/- 1-DSO
Differentiation
B
Energy phenotype profile
AEROBIC
ENERGETIC
QUIESCENT
GLYCOLYTIC
OCR (pmol/min)
ECAR (pmol/min)
Differentiated
Undiff
Con
1-DSO
C
Basal
Maximal
Spare respiratory capacity
OCR (pmol/min)
Con
Con+Eto
1-DSO
1-DSO+Eto
D
Differentiated
Con
1-DSO
PPARγ
PGC1α
CPT1A
FABP4
CypA
Primary ASCs
E
Kinetic graph
Oligo
FCCP
R/A
Con
n6-FA
n6-FA+1-DSO
OCR (pmol/min)
Time (minutes)
F
Energy phenotype profile
AEROBIC
ENERGETIC
QUIESCENT
GLYCOLYTIC
Con
n6-FA
n6-FA+1-DSO
OCR (pmol/min)
ECAR (pmol/min)
G
Basal
Maximal
Spare respiratory capacity
OCR (pmol/min)
Con
n6-FA
n6-FA+1DSO
H
SLC2A1
CD36
SLC16A1
P3H3
P3H4
GLS
P4HA1
SLC1A5
PLOD1
SERPINH1
PLPP3
SPTLC1
SPTLC2
GBA1
ASAH1
KDSR
VDAC1
SPHK2
SCARB2
NPC1
HEXB
PSAP
GNAI1
GNAI2
GNAI3
PTDSS2
CHPT1
CEPT1
NDUFA9
NDUFB9
NDUFA13
NDUFB7
ATP5PD
NDUFC2
NDUFS7
NDUFS3
UQCRFS1
NDUFS1
NDUFV2
SLC25A5
NDUFV1
SCARB1
EBP
LRP1
APOH
LPL
VDAC1
MGAT1
DHCR7
GNPAT
GPAM
EFTUD2
HNRNPM
TMED10
DHX9
U2AF2
SRSF1
DHX15
U2AF1
SRSF6
PRPF8
SF3B1
Fibroblasts metabolism
Sphingolipid metabolism
Biosynthesis and turnover of 1-Deoxy sphingoid bases
S1P Receptor signalling
Kennedy pathway from sphingolipids
Electron transport chain
Oxidative phosphorylation
Mitochondrial complex-I assembly
Cholesterol metabolism
Triglyceride synthesis
mRNA processing
n6
n6 + 1-DSO
I
UGP2
PHGDH
PSPH
PGM1
GPI
LDHA
TPI1
PGAM1
ENO1
LDHB
PGK1
ALDOA
PDHA1
PC
MDH1
MDH2
DLAT
DLD
GOT1
CS
ACLY
DLST
ACO1
IDH3A
IDH3B
IDH3G
ACO2
ME1
HADHB
LIPE
ECHS1
ACSS2
ACADL
ECI1
ACADM
HADH
ACADS
CRAT
ACAA2
FASN
ECHDC1
ACACA
ACACB
AKT2
PRKACA
FDPS
DBI
FABP4
FABP5
Fibroblasts metabolism
Glycolysis
Gluconeogenesis
TCA Cycle
Deficiency Of Pyruvate Dehydrogenase Complex
Lipid Metabolism
Fatty Acid Beta Oxidation
Fatty Acid Biosynthesis
Fatty Acid Transporters
n6
n6 + 1-DSO

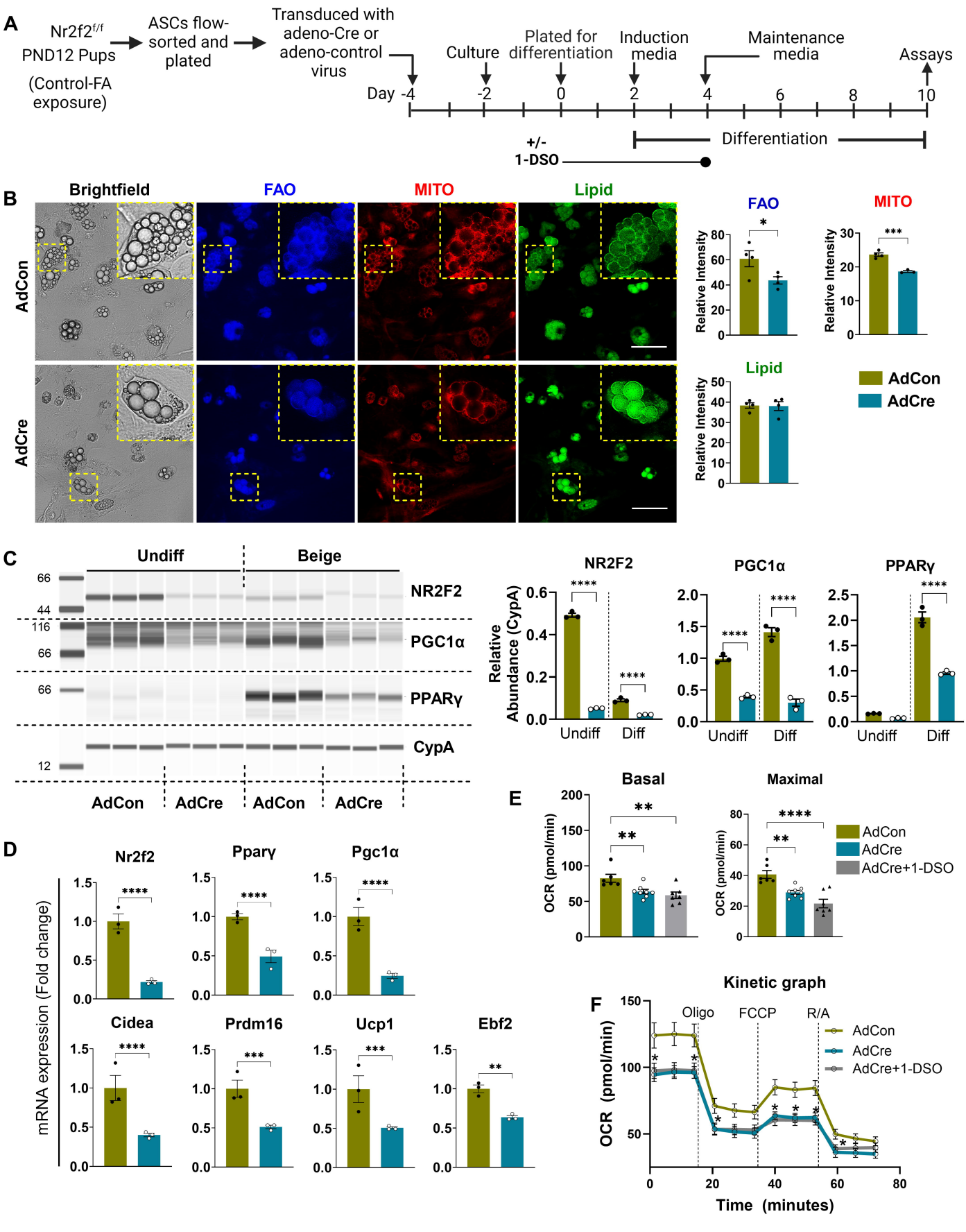
A
Nr2f2f/f
PND12 Pups
(Control-FA exposure)
ASCs flow-sorted and plated
Transduced with adeno-Cre or adeno-control virus
Culture
Plated for differentiation
Induction media
Maintenance media
Assays
Day -4
-2
0
2
4
6
8
10
Differentiation
+/-
1-DSO
B
Brightfield
FAO
MITO
Lipid
AdCon
AdCre
Relative Intensity
AdCon
AdCre
C
Undiff
Beige
NR2F2
PGC1α
PPARγ
CypA
AdCon
AdCre
AdCon
AdCre
Relative Abundance (CypA)
Undiff
Diff
D
mRNA expression (Fold change)
Nr2f2
Pparγ
Pgc1α
Cidea
Prdm16
Ucp1
Ebf2
E
Basal
Maximal
OCR (pmol/min)
AdCon
AdCre
AdCre+1-DSO
F
Kinetic graph
Oligo
FCCP
R/A
OCR (pmol/min)
Time (minutes)

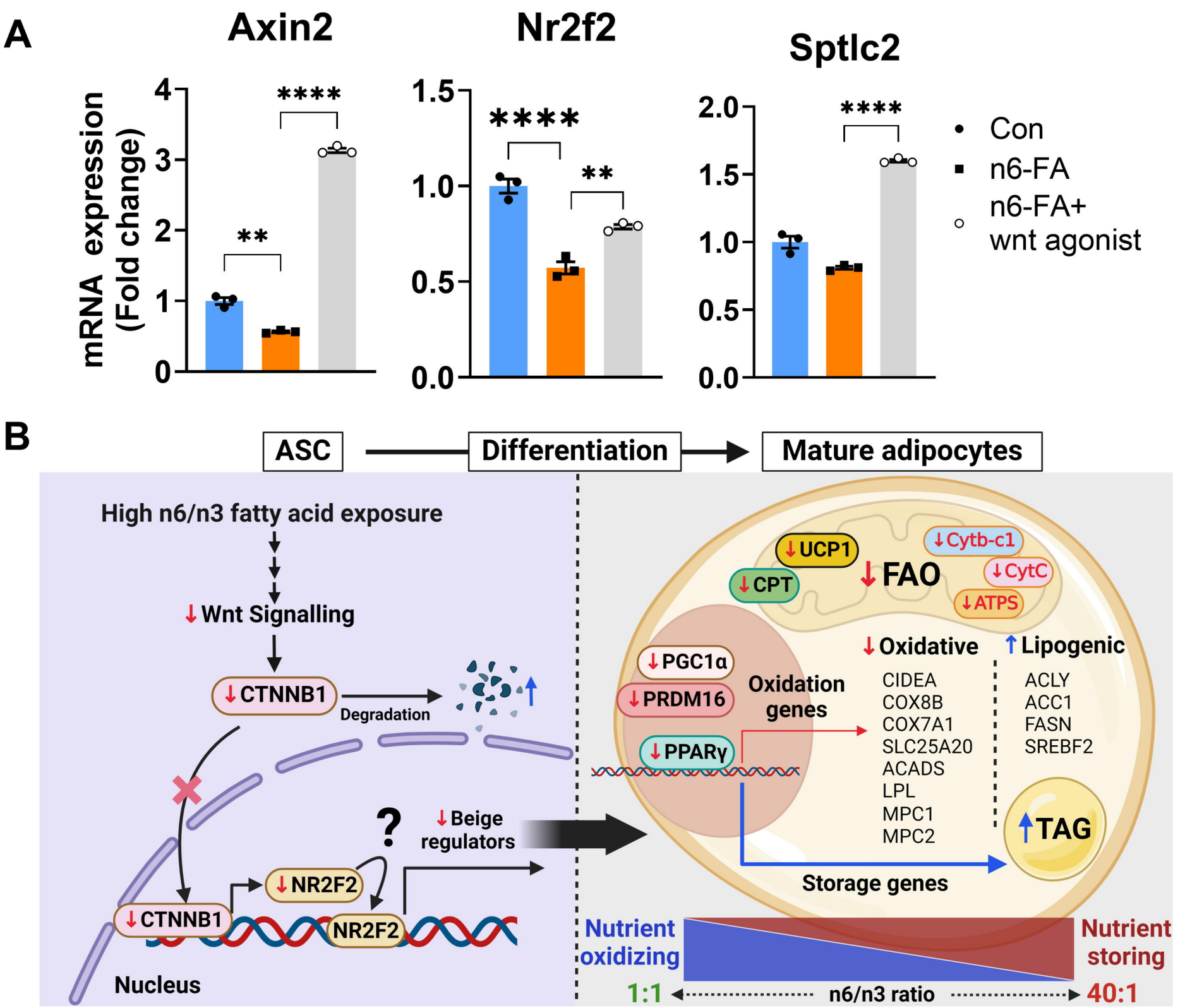

*Red and blue colored arrows indicate effect of n6-FA exposure
Red arrow- Decrease, Blue arrow- Increase.